Production and characterization of different variants of Myriococcum thermophilum cellobiose dehydrogenase with the aim of improving cofactor binding and kinetic stability

Ilić, Mario

Master's thesis / Diplomski rad

2022

Degree Grantor / Ustanova koja je dodijelila akademski / stručni stupanj: **University of Zagreb, Faculty of Food Technology and Biotechnology / Sveučilište u Zagrebu, Prehrambeno-biotehnološki fakultet**

Permanent link / Trajna poveznica: https://urn.nsk.hr/urn:nbn:hr:159:847876

UNIVERSITY OF ZAGREB
FACULTY OF FOOD TECHNOLOGY AND BIOTECHNOLOGY

GRADUATE THESIS

Zagreb, February 2022

Mario Ilić

PRODUCTION AND CHARACTERIZATION OF DIFFERENT VARIANTS OF *Myriococcum thermophilum* CELLOBIOSE DEHYDROGENASE WITH THE AIM OF IMPROVING COFACTOR BINDING AND KINETIC STABILITY

This study was carried out at the Department of Food Science and Technology, BOKU – University of Natural Resources and Life Sciences, Vienna under supervision of Roland Ludwig, associate professor with the assistance of Erik Breslmayr, PhD and PhD candidate Lan Zhang, MSc.

This work was conducted within the Life Science Project LS17-069 “Diaziridine-FAD: A stable cofactor for biocatalysts and a molecular probe” funded by the Vienna Science and Technology Fund (principal investigator Roland Ludwig, PhD, Associate professor).

I would like to thank associate professor Roland Ludwig for accepting my application and giving me the opportunity to conduct my Master thesis in his inspiring working group. I would also like to thank Erik Breslmayr, Ph.D. for his supervision, instructive input and at the same time freedom to work on my own. Special thanks go to Lan Zhang, MSc. for all the help and patience during the ups and downs of the experimental work. Of course, I would like to thank the rest of the group for all the help, support and encouraging atmosphere during my stay in Vienna (Institute of Food Technology, University of Natural Resources and Life Sciences, Vienna).

Moreover, I would like to thank full professor Tonči Rezić for his helpful advice and supervision (Department of Biochemical Engineering, Faculty of Food Technology and Biotechnology, Zagreb).

Također bih se zahvalio svim zaposlenicima Laboratorija za biokemijsko inženjerstvo, industrijsku mikrobiologiju i tehnologiju piva i slada na savjetima, prenesenom znanju i uvijek ugodnoj radnoj atmosferi.

Hvala kolegama i prijateljima na nezaboravnim studentskim danima, a posebno osobama koji su u ovom periodu bile dio mog života.

Na kraju, od srca se zahvaljujem svojoj obitelji i roditeljima na strpljenju i podršci za vrijeme studiranja.

BASIC DOCUMENTATION CARD

Graduate Thesis

University of Zagreb
Faculty of Food Technology and Biotechnology
Department of Biochemical Engineering
Laboratory for Biochemical Engineering, Industrial Microbiology and Malting and Brewing Technology

Scientific area: Biotechnical Sciences
Scientific field: Biotechnology

Graduate university study programme: Bioprocess Engineering

PRODUCTION AND CHARACTERIZATION OF DIFFERENT VARIANTS OF *Myriococcum thermophilum* CELLOBIOSE DEHYDROGENASE WITH THE AIM OF IMPROVING COFACTOR BINDING AND KINETIC STABILITY

Mario Ilić, univ. bacc. ing. biotechn.
0058210593

Abstract: Biosensors are being extensively used in the healthcare sector but mostly in blood glucose monitoring for early diagnosis of diabetes. The use of enzymes as biological recognition elements is hampered in many ways, e.g., by insufficient communication between enzyme and electrode, low activity and stability. Cellobiose dehydrogenase (CDH) is a flavocytochrome enzyme that in native wild-type form shows efficient direct electron transfer (DET). To alter FAD cofactor binding and kinetic stability, mutations were introduced into the *Myriococcum thermophilum* CDH gene by site-directed mutagenesis. Variants were expressed in X-33 *Pichia pastoris* cells, purified and characterized. With an increased specific activity, catalytic efficiency, heme reduction rate and increased melting temperatures in pH range 5.0-8.0 the T306I variant seems to be the most promising variant for further investigation.

Keywords: *biosensors, Myriococcum thermophilum, cellobiose dehydrogenase, DET, kinetic stability*
Thesis contains: 75 pages, 39 figures, 19 tables, 50 references, 0 supplements
Original in: English
Graduate Thesis in printed and electronic (pdf format**) form is deposited in:** The Library of the Faculty of Food Technology and Biotechnology**,** Kačićeva 23, Zagreb.

Mentor: Tonči Rezić, PhD, Full professor
Co-mentor: Roland Ludwig, PhD, Associate professor
Technical support and assistance: Erik Breslmayr, PhD and Lan Zhang, Msc

Reviewers:
1. Blaženka Kos, PhD, Full professor
2. Tonči Rezić, PhD, Full professor
3. Roland Ludwig, PhD, Associate professor, BOKU, Vienna
4. Jasna Novak, PhD, Full professor (substitute)

Thesis defended: February 04, 2022

TEMELJNA DOKUMENTACIJSKA KARTICA

Diplomski rad

Sveučilište u Zagrebu
Prehrambeno-biotehnološki fakultet
Zavod za biokemijsko inženjerstvo
Laboratorij za biokemijsko inženjerstvo, industrijsku mikrobiologiju i tehnologiju slada i piva

Znanstveno područje: Biotehničke znanosti
Znanstveno polje: Biotehnologija

Diplomski sveučilišni studij: Bioprocesno inženjerstvo

PROIZVODNJA I KARAKTERIZACIJA MUTANATA *Myriococcum thermophilum* CELOBIOZA DEHIDROGENAZE S CILJEM POVEĆANJA VEZANJA KOFAKTORA I KINETIČKE STABILNOSTI

Mario Ilić, univ. bacc. ing. biotechn.
0058210593

Sažetak: Biosenzori se uvelike koriste u zdravstvenom sektoru, a najveću primjenu pronalaze u praćenju i kontroli šećera glukoze oboljelih od dijabetesa. Uporaba enzima u biosenzorima je ograničena nedovoljno efikasnim direktnim prijenosom elektrona na elektrodu, niskom specifičnom aktivnosti i stabilnosti kroz duži vremenski period. Celobioza dehidrogenaza (CDH) je flavocitokrom koji u svojoj izvornoj formi ima mogućnost direktnog prijenosa elektrona (DET). S ciljem povećanja vezanja FAD koenzima i kinetičke aktivnosti, uvedene su mutacije u CDH gen izoliran iz askomicete *Myriococcum thermophilum.* Enzimi proizvedeni u soju kvasca *Pichia pastoris* X-33 su pročišćeni i karakterizirani. Mutant T306I pokazuje zadovoljavajuća svojstva (povećanu specifičnu aktivnost, kinetičku efikasnost, brzinu redukcije hema i temperaturu prijelaza) u području pH vrijednosti 5,0-8,0, stoga je potrebno provesti dodatna istraživanja korištenjem mutanta T306I.

Ključne riječi: *biosenzori, Myriococcum thermophilum, celobioza dehidrogenaza, DET, kinetička stabilnost*

Rad sadrži: 75 stranica, 39 slika, 19 tablica, 50 literaturnih navoda, 0 priloga
Jezik izvornika: engleski
Rad je u tiskanom i elektroničkom (pdf format) obliku pohranjen u: Knjižnica Prehrambeno-biotehnološkog fakulteta, Kačićeva 23, Zagreb

Mentor: prof. dr. sc. Tonči Rezić
Komentor: izv.prof.dr.sc. Roland Ludwig
Pomoć pri izradi: dr. sc. Erik Breslmayr i Msc. Lan Zhang

Stručno povjerenstvo za ocjenu i obranu:
1. prof. dr. sc. Blaženka Kos
2. prof. dr. sc. Tonči Rezić
3. izv. prof. dr. sc. Roland Ludwig, BOKU, Vienna
4. prof. dr. sc. Jasna Novak (zamjena)

Datum obrane: 04. veljače 2022.

Table of Contents

1. INTRODUCTION

A biosensor is a compact analytical device comprising of a biological or biologically derived sensitive recognition element (receptors, enzymes, antibodies, nucleic acids, microorganisms, or lectins) integrated or associated with a physio-chemical transducer. Together, they detect the concentration of an analyte, or group of analytes to a measurable response. Biosensors are being extensively used in the healthcare sector in cholesterol testing and drug discovery, but mostly in blood glucose monitoring for early diagnosis of diabetes and diabetes control (Nandini et al., 2016). The rising prevalence of diabetes as stated by the International Diabetes Federation is about 8.0 %, annually, estimating over 590 million people to acquire diabetes till 2035, hence promoting considerable growth of the market over the next period (Grand View Research, 2021).

However, a major barricade in electrochemical systems lies in the electrical communication between the biological recognition element, such as a redox protein, and signal transducers, here the electrode material. One proposed way to achieve efficient electrical communication is based on the direct electron transfer of proteins and application of third-generation biosensors. In third-generation biosensors, electrons are transferred directly from the enzyme to the electrode without any intermediates such as redox mediators (Zhang and Li, 2004).

Cellobiose dehydrogenase (CDH) is a flavocytochrome which belongs to the restricted number of oxidoreductases that in their native wild-type form show efficient direct electron transfer (DET) between the active site and an electrode surface (Scheiblbrandner and Ludwig, 2019). CDHs are composed of two domains: a heme *b*-binding cytochrome domain and a FAD-binding dehydrogenase catalytic domain which are connected by a flexible linker. A good interaction of the cytochrome domain with the active site cofactor (FAD) is important to obtain high IET (interdomain electron transfer) and DET rates and consequently a high current density for glucose biosensors (Kracher and Ludwig, 2016).

The goal of this thesis was to produce and characterize different variants of *Myriococcum thermophilum* CDH with hopefully improved cofactor binding and kinetic stability. Mutations were introduced into the *Myriococcum thermophilum* CDH gene by site-directed mutagenesis, expressed in X-33 *Pichia pastoris* cells.

2. THEORY

2.1. GMC-OXIDOREDUCTASES

The glucose-methanol-choline (GMC)-oxidoreductases are a family of functionally diverse proteins first described almost 40 years ago. Sequence similarities of *Drosophila melanogaster* glucose dehydrogenase, *Escherichia coli* choline dehydrogenase, *Aspergillus niger* glucose oxidase and *Hansenula polymorpha* methanol oxidase share a common structural fold around the flavin adenine dinucleotide (FAD) cofactor, also known as Rossmann fold or the βαβ mononucleotide-binding motif. These four are similar throughout their primary sequence, recognized as homologous proteins and therefore named the glucose-methanol-choline (GMC) oxidoreductase family (Cavener, 1992). GMC-oxidoreductases catalyze reactions such as glucose oxidation to gluconolactone by glucose dehydrogenase or short-chain aliphatic alcohols oxidation (i.e., methanol) to the respective aldehyde by alcohol oxidase (Ozimek et al., 2005).

Since then, many more enzymes from different species, including yeasts, filamentous fungi, bacteria and insects have been identified as members of this group. From a higher-scale application point of view, GMC oxidoreductases from fungal sources have attracted the most attention in, e.g., biosensors and the food industry. Furthermore, fungal members such as aryl-alcohol oxidoreductase, pyranose dehydrogenase, pyranose oxidase and cellobiose dehydrogenase are relevant for biomass utilization (Sützl et al., 2019).

2.2. CELLOBIOSE DEHYDROGENASE

Cellobiose dehydrogenase (CDH, EC 1.1.99.18) is an extracellular flavocytochrome enzyme secreted by white and brown rot, plant-pathogenic and composting fungi from Basidiomycota and Ascomycota under cellulolytic culture conditions (Zamocky et al., 2006). CDH is listed in the carbohydrate active enzymes database (CAZy), forming the first of four subfamilies of the CAZy auxiliary activity families (AA3_1). It is based on its function to support polysaccharide depolymerization by lytic polysaccharide monooxygenase (LPMO). The discovery of LPMO in 2010 and subsequent studies revealed CDH's natural function - the reduction of LPMO via extracellular electron transfer (Scheiblbrandner and Ludwig, 2019). As a cellulolytic monooxygenases' activator, which increases the accessibility of crystalline cellulose surfaces for hydrolases, CDHs hold great potential to improve the efficiency of

commercial enzyme mixtures for biomass processing and biofuel production (Zamocky et al., 2006).

Since CDH was discovered in 1974 in the exo-enzyme system of the wood-degrading fungus *Phanerochaete chrysosporium* (Westermark and Eriksson, 1974)**,** a plethora of studies have been conducted. Some of the reported CDH functions are cellulose and lignin depolymerization, prevention of cellulose repolymerization or manganese peroxidase auxiliary role (Cameron and Aust, 2001). The extracellular enzyme manganese peroxidase is believed to degrade lignin by a hydrogen peroxide-dependent oxidation of Mn^{2+} to the reactive Mn^{3+} that attacks the lignin, and this reaction is supported by CDH (Hildén et al., 2000). Moreover, hydroxyl radical hypothesis represents CDH's ability to produce hydrogen peroxide and ferrous ion complexes, important in a Fenton reaction, which are able to oxidize a wide range of organic substrates (Kremer and Wood, 1992). Of all the above, after the discovery of direct electron transfer, CDH's role as an electron donor for LPMO and application in biosensor industry became favored and intensively studied.

2.3. CLASSIFICATION

CDHs are classified into four phylogenetic groups (Figure 1). Class I CDH sequences are found in Basidiomycota whereas CDH sequences from Class II, Class III, and Class IV are found only in Ascomycota. Class I CDHs favor cellulose as a substrate and bind, presumably via a cellulose binding-site, on the surface of the DH domain which is different from the active-site and not present in other CDH classes. Some CDHs in Class II are carrying a C-terminal carbohydrate-binding module (CBM) and are thus classified into CDH IIA (with a CBM) and CDH IIB (without a CBM). Some sequences from the CDH III clade also show a CBM, but only a small subgroup (Sützl et al., 2019). Genes from the recently discovered Class IV, evolutionary furthest related to the other CDH classes, are lacking a CYT domain and strictly show a dehydrogenase (DH) domain only. Consequently, it suggests a different physiological role and the loss of its ability for direct electron transfer (DET) (Scheiblbrandner and Ludwig, 2019).

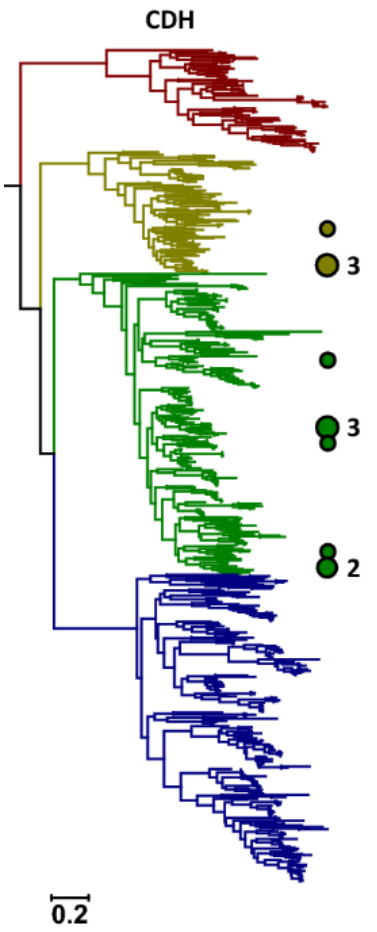

	Phylum	No. of sequences	Characterized [PDB]	Mean % seq. ident.
CDH IV	Ascomycota	83	———	58 ± 8
CDH I	Basidiomycota	99	*P. chrysosporium* [1NAA][1] *G. subvermispora*[2] *T. cinnabarina*[3] *T. Versicolor*[4]	59 ± 8
CDH II	Ascomycota	245	*D. saubinetii*[5] *N. crassa* [4QI7][6] *A. atrobrunnea*[5] *C. hotsonii* [4QI5][6] *S. bisbyi*[5] *H. haematostroma*[5] *C. thermophilum*[5] *H. insolens*[7]	56 ± 7
CDH III	Ascomycota	250	———	50 ± 9

Figure 1. Maximum likelihood tree of the dehydrogenase domains in the cellobiose dehydrogenase (CDH) cluster (adapted from Sützl et. al, 2019)

2.4. STRUCTURE OF CDH

Cellobiose dehydrogenase consists of a catalytically active DH domain and an electron-transferring cytochrome (CYT) domain connected by a linear papain-sensitive flexible linker. The linker typically contains from 15 to 33 amino acids (Kracher and Ludwig, 2016). The supposed mobility of the CYT domain has been considered a key factor for CDH's function but also because of complex structure, prevented the crystallization and X-ray structure elucidation of CDH. After firstly indicated „cigar-shaped" conformation and still unclear details regarding its dynamic behavior (Lehner et al., 1996), the crystal structures of the individual CYT (Hallberg et al., 2000) and DH (Hallberg et al., 2002) domains were detected. The structures provided a strong basis for the interdomain electron transfer, important for biochemical and bioelectrochemical studies (Zamocky et al., 2006).

2.4.1. Cytochrome domain (CYT)

As mentioned, the crystal structure of the CYT domain from *Pc*CDH was described in 2000. The polypeptide has an ellipsoidal antiparallel β-sandwich topology forming a compact globular structure with approximate dimensions of 30× 36×47 Å (Hallberg et al., 2000). The CYT domain features a ligation with methionine and histidine, which is not common for *b*-type cytochromes but for *c*-type cytochromes. Only very few *b*-type cytochromes are known to have this unusual ligation, including cytochrome *b*562, located in the periplasm of *E. coli* (Mathews et al., 1979). Mutational studies have confirmed that methionine and histidine are the axial ligands of the heme *b* iron in *Pc*CDH. Interestingly, replacing either of Met65/His163 ligands by alanine resulted in a loss of IET while remaining the ability to oxidize cellobiose in the presence of 2,6-dichlorophenolindophenol (DCIP) as an electron acceptor (Rotsaert et al., 2001).

2.4.2. Dehydrogenase domain (DH)

The catalytic domain of CDH belongs to the glucose–methanol–choline (GMC) oxidoreductase superfamily with FAD as the prosthetic group (Sützl et al, 2019). Molecular masses are usually within 90 to 100 kDa and the mass percentage of its glycosylation is around 10 % (Hallberg et al., 2000). The overall structure of the DH domain from *Pc*CDH was described as "peanut-shaped with dimensions of ~72×57×45 Å and it is divided into two subdomains: a substrate-binding (S) and a flavin-binding, catalytic (F) subdomain. The main structural feature of the S subdomain is a central twisted, seven-stranded β-sheet with three α helices on one side of the sheet, and the active site on the other side. The F subdomain mainly consists of the Rossmann fold, which is typical for NAD(P)- and FAD-dependent enzymes (Hallberg et al., 2002). The FAD moiety, which is non-covalently bound to the enzyme and shows a butterfly-like bending in *P. chrysosporium* DH, is as well buried in the interior of the enzyme, approximately 12 Å below the protein surface (Kracher and Ludwig, 2016).

2.4.3. Full-length structure of CDH

The mobility of the CYT domain in CDH is necessary for the interdomain electron transfer and is also the reason why the crystallization of the full-length CDH was so difficult to discover. It was until 2015, when the structures of two full-length CDHs from *Myriococcum thermophilum* and *Neurospora crassa* were published. This acknowledgment leads to a better

understanding of the structure-function relationship of CDH and the role of its CYT domain as a built-in redox mediator, which transfers electrons to external electron acceptors like LPMO (Tan et al., 2015).

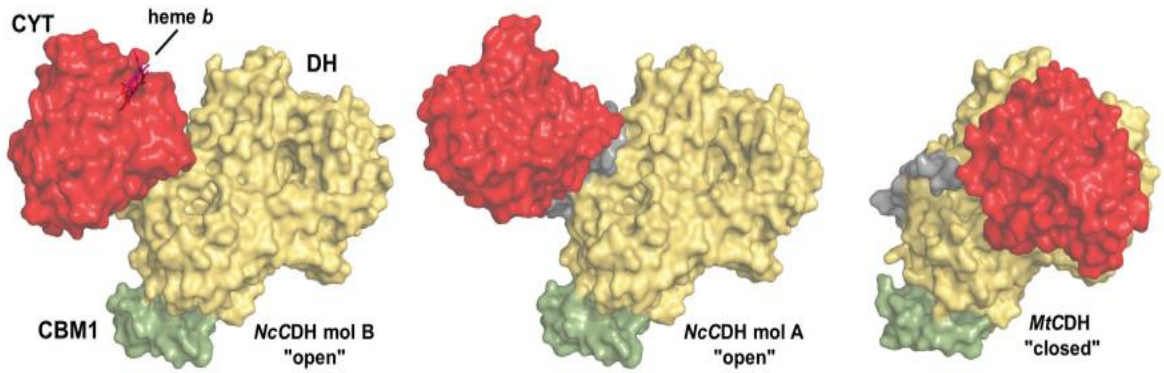

Figure 2. Crystal structures of full-length CDHs from *Neurospora crassa* (PDB: 4QI7) and *M. thermophilum* (PDB: 4QI6) (adapted from Kracher and Ludwig, 2016)

Relative orientations of the cytochrome (CYT) domains (red), the dehydrogenase (DH) domains (yellow) and the linker peptides (grey) in the "open" state of two *N. crassa* CDHs in comparison to the "closed" state of *M. thermophilum* CDH are shown in the Figure 2. While the closed conformation of CDH favors interaction between the redox centers, the open conformation may allow the interaction of CYT with external electron acceptors, such as LPMO (Kracher and Ludwig, 2016), also shown in Figure 2. Following substrate oxidation, electrons are transferred sequentially from the reduced flavin to the heme cofactor and eventually to a suitable electron acceptor (Figure 3).

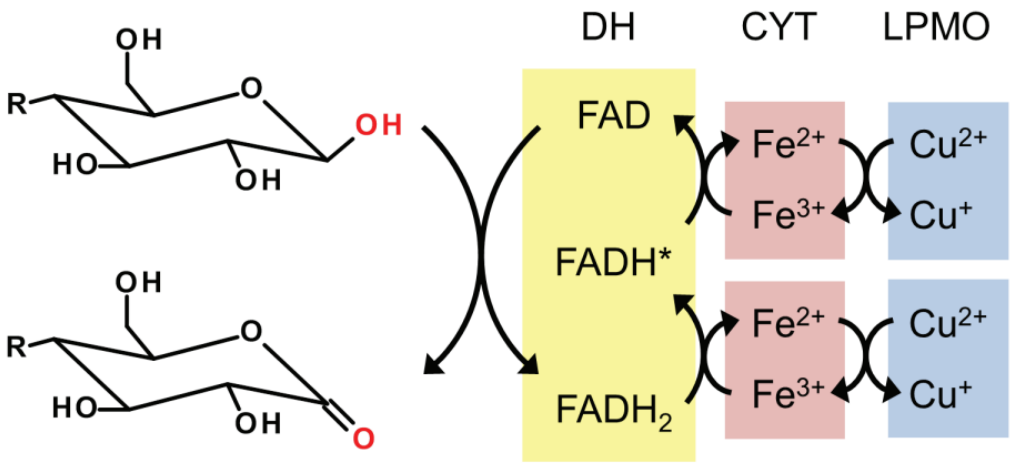

Figure 3. Electron-chain model for electron transfer in CDH (adapted from Heriksson et al., 2000)

2.5. GMC-OXIDOREDUCTASE APPLICATIONS

Because of their attractiveness and promising applications in biomass utilization, food industry, biofuel cell development or biosensors, fungal GMC-oxidoreductases are the best characterized enzymes within this superfamily.

LPMOs are unique in the way that they can „attack" polysaccharides organized in recalcitrant structures (crystalline cellulose or chitin; hemicellulose complexes) and for its ability to act on surfaces - they cleave a polysaccharide chain while this chain is in a crystalline context (Bissaro et al., 2018). As already stated, the flavin and heme cofactor containing cellobiose dehydrogenase is an activator for cellulolytic monooxygenases, which increase the accessibility of crystalline cellulose surfaces for hydrolases. Consequently, CDHs hold great potential to improve the efficiency of commercial enzyme mixtures for lignocellulose degradation and therefore biochemicals and biofuel production.

From glucose oxidase (GOx), pyranose dehydrogenase (PDH), and the already mentioned cellobiose dehydrogenase, many GMC-oxidoreductases find their place and potential in the food industry. GOx is Generally Regarded as Safe (GRAS status) and it is a core of many industrial processes, such as dry egg powder, gluconic acid and wine production, but it is also used in baking industry. In the wine industry, i.e., GOx reduces the amount of available glucose, in order to decrease final alcohol concentration (Wong et al., 2008). Pyranose dehydrogenase (PDH) of the mushroom *Agaricus meleagris* is used in the C-2 specific conversion of D-galactose into pure D-fructose or prebiotic sugar D-tagatose (Sygmund et al., 2008). CDHs have great potential for application in the dairy industry and other areas where low-concentration products are produced. Some of target products are lactose-reduced or lactose-free milk with lactose concentrations in the range of 0.1-1.5 g L^{-1}, whey drinks and products such as cream soups and cream sauces with lactose concentration below 0.1 g L^{-1}. The detection of low lactose concentrations is of great importance for lactose intolerant people and dairy and milk industry, respectively (Stoica et al., 2006). A great example of CHD as a recognition element in biosensors is the third-generation lactose biosensor launched by DirectSens GmbH in 2017, which is able to detect very low lactose concentrations (0.1 g L^{-1}) in lactose-reduced milk products (DirectSens, 2021).

Another interesting application possibility is in enzymatic fuel cells (EFCs). GMC-oxidoreductases show vast potential in EFCs, which can produce electrical energy from glucose present in human sweat and saliva, used as a potential power source for skin-worn electronic

devices. Such products could find application in non-invasive autonomous biodevices with great benefits for biomedical monitoring (Falk et al., 2014).

2.5.1. Biosensors

A biosensor is a compact analytical device or unit containing a biological or biologically derived sensitive recognition element (receptors, enzymes, antibodies, nucleic acids, microorganisms and lectins) integrated or associated with a physio-chemical transducer. In short, the recognition element differentiates the target molecules, a transducer converts the biorecognition event into a measurable signal and a signal processing system converts the signal into a readable form (Yoo and Lee, 2010). The global biosensors market size was valued at 22.4$ billion in 2020 and is expected to increase at a compound annual growth rate (CAGR) of 7.9 % from 2021 to 2028 (Grand View Research, 2021). Biosensors are being extensively used in the healthcare sector in cholesterol testing and drug discovery, but mostly in blood glucose monitoring for early diagnosis of diabetes (Nandini et al., 2016). The rising prevalence of diabetes as stated by the International Diabetes Federation is about 8.0 %, annually, estimating over 590 million people to acquire diabetes until 2035, hence promoting considerable growth of the market over the next period (Grand View Research, 2021).

Throughout history, several approaches for diagnosis of diabetes such as gas chromatography/mass spectrometry (GC/MS), capillary zone electrophoresis (CZE) and high-performance liquid chromatography have been investigated. Anyhow, these methods demand expensive equipment and complicated operations which don't get along with the patient's needs who have to test their blood periodically, sometimes several times per day. As a great motive to lower the cost and simplify usage - accurate, repeatable, time-saving and cost-effective biosensor devices are used as determination method of glucose in blood (Bollella et al., 2017). Electrochemical enzymatic glucose biosensors are divided into three groups depending on the electrochemical communication between the enzyme and the electrode (Figure 4).

2.5.1.1. First-generation biosensors

In biosensors of the first generation, electrons are transferred to molecular oxygen. The most widely used enzyme for this setup is *Aspergillus niger* GOx and these biosensors measure either the decrease of oxygen or the increase of the produced hydrogen peroxide. Since oxygen-based devices depend on the availability of oxygen as an electron acceptor, they are affected by variations in oxygen concentrations (Wang, 2002). Even though hydrogen peroxide formation

is simple to detect and measure, hydrogen peroxide contributes to the deactivation of enzymes such as GOx, which consequently decreases the sensors stability.

2.5.1.2. Second-generation biosensors

The limitations in first-generation sensors were overcome by using mediated glucose biosensors. For this kind of biosensors, improvements were achieved by replacing oxygen with non-physiological electron acceptors – redox mediators, which can transfer electrons from the enzyme to the surface of the electrode. Instead of hydrogen peroxide, a redox mediator is reduced and then reoxidized by the electrode, providing a detectable signal. This kind of transfer is called mediated electron transfer (MET) and PQQ-GDHs and FAD-GDHs are commonly used as a recognition element. Some of the commonly used redox mediators are ferricyanide, ferrocene, quinines, thionine and others. Ferrocenes show best results since they don't react with oxygen, are stable in oxidized and reduced forms and are stable over a large pH range (Yoo and Lee, 2010).

2.5.1.3. Third-generation biosensors

In third-generation biosensors, electrons are transferred directly from the enzyme to the electrode without any intermediate stages. Enzymes are capable of DET and are therefore independent of external electron mediators. However, the electron transfer rate is restricted by the electron transfer distance. Since the active site of most enzymes used in biosensors isn't close to the surface of the enzyme, a direct electrical coupling of the enzymatic activity with the electrode is hard to achieve (Pereira et al., 2018). A limited number of enzymes can perform DET efficiently and one of them is cellobiose dehydrogenase (CDH) from various fungal sources (Scheiblbrandner and Ludwig, 2019).

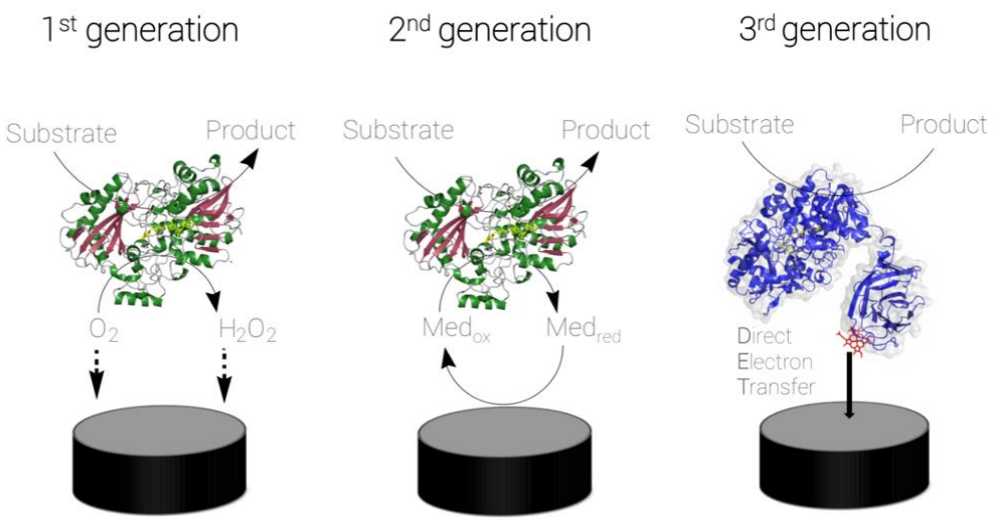

Figure 4. Three generations of biosensors according to their electron-coupling (adapted from DirectSens, 2021)

2.5.2. Direct electron transfer capabilities of CDH

Cellobiose dehydrogenase (CDH) is a flavocytochrome which belongs to the restricted number of oxidoreductases that in their native wild-type form show efficient direct electron transfer (DET) between the active site and an electrode surface (Scheiblbrandner and Ludwig, 2019).

The electron transfer pathways between the dehydrogenase domain of CDH (DH_{CDH}) and an electrode can be achieved along different paths as illustrated in Figure 5. In the first reaction, the sugar substrate is oxidized at the C1 position into its corresponding lactone and simultaneously the FAD in the active site of the DH_{CDH} is fully reduced to $FADH_2$-DH_{CDH} (Equation 1). When CDH is immobilized on the electrode surface and in the absence of any competing e− acceptors, the reoxidation of the reduced enzyme can be summarized as follows (Equation 2). Hence, there is no $2e^-/2H^+$ acceptor such as quinone, electron transfer is followed by a first electron transfer (ET) step to the electrode and a second IET step delivering the second electron from DH_{CDH} to the cytochrome domain of CDH (CYT_{CDH}) (Equation 3). Lastly, the second electron is delivered to the electrode (Equation 4) (Ludwig et al., 2013).

$$sugar + FAD - DH_{CDH} \rightarrow lactone + FADH_2 - DH_{CDH} \quad [1]$$

$$FADH_2 - DH_{CDH} - Fe^{3+} - CYT_{CDH} \xrightarrow{1st\ IET\ step} FADH \cdot\ DH^{-}_{CDH} - \ Fe^{2+} - CYT_{CDH} + H^{+} \quad [2]$$

$$FADH \cdot\ DH^{-}_{CDH} - \ Fe^{2+} - CYT_{CDH} \xrightarrow{1st\ DET\ +\ 2nd\ IET\ step} FAD - DH_{CDH} - \ Fe^{2+} - CYT_{CDH} + H^{+} + e^{-}\ (electrode) \quad [3]$$

$$FADH \cdot\ DH^{-}_{CDH} - \ Fe^{2+} - CYT_{CDH} \xrightarrow{1st\ DET\ +\ 2nd\ IET\ step} FAD - DH_{CDH} - \ Fe^{2+} - CYT_{CDH} + H^{+} + e^{-}\ (electrode) \quad [4]$$

Reactions leading to the direct electron transfer with CDH immobilized on the electrode surface with a CYT domain as an electron shuttle (Figure 5):

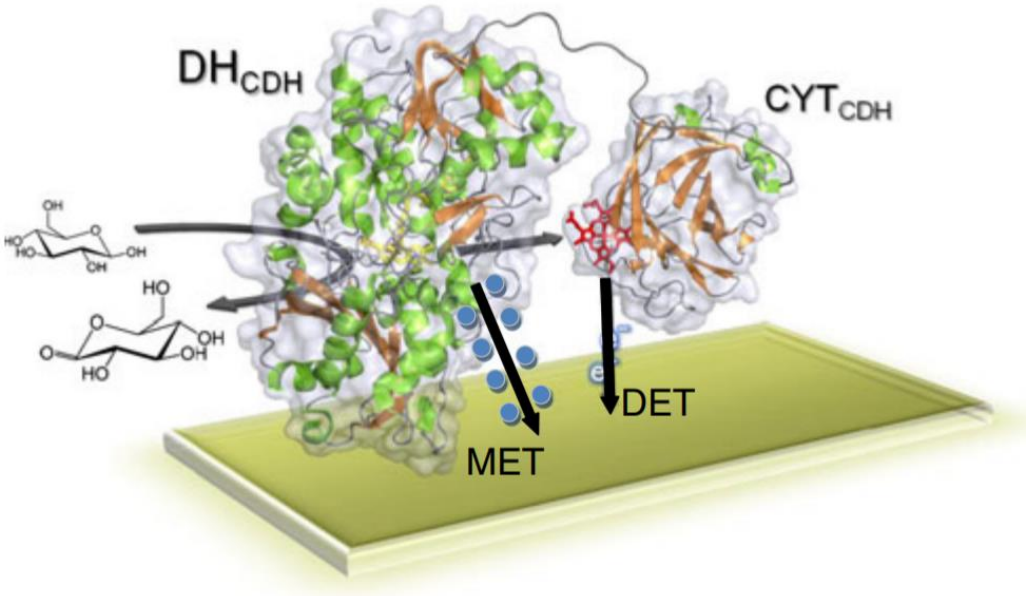

Figure 5. Electron transfer between both CDH domains and the terminal electron acceptor (adapted from Ludwig et al., 2013)

There are two perspectives contemplated and used to optimize DET from CDH to electrodes. The first one is based on the development of new electrode nanomaterials, nanostructures and chemically modified electrode surfaces to increase the effective surface area available for CDH binding, or to increase the DET rate by appropriate orientation of the enzyme

on the surface. The second, biochemical approach uses modifications of the enzyme or the reaction cascade to increase the current of CDH-based electrodes (Ludwig et al., 2013).

Latest attempts in the design of third-generation CDH-based glucose biosensors resulted in an engineered *Corynascus thermophilum* CDH variant with altered substrate specificity beneficial for glucose catalysis. The amino acid substitution from a cysteine to a tyrosine in the substrate binding region improved the sensitivity and limit of detection of a graphite adsorbed *Ct*CDH for glucose detection and altered the enzyme stability, respectively (Ortiz et al., 2017). Another biochemical approach was shown from Geiss et al. (2021), who described two mechanisms contributing to turnover stability. One of these was the replacement of methionine side chains prone to oxidative damage and in the electrochemical long-term measurement setup, one variant (M409S) was confirmed to be 20 % more stable compared to the wild-type.

2.6. EXPRESSION SYSTEM

Compared with bacteria, yeast cells have significant advantages including growth rate, posttranslational modification, secretory expression, and easy genetic manipulation - linearized foreign DNA can be inserted in a chromosome in high efficiency via crossing over recombination phenomena to generate stable cell lines (Karbalaei et al., 2020).

The yeast *Saccharomyces cerevisiae* is a model organism widely used to study cell biological processes because of its easy genomic manipulation and its close relatedness to higher eukaryotes (Buser, 2010). It combines the advantages of eukaryotic expression with the ability to fold complex proteins, and with high productivity and low-cost media requirements - correlated with microbial systems. However, the expression proteins of this commonly used yeast are often N and O-hyperglycosylated, which could affect protein immunogenicity (Rasala and Mayfield, 2014). With the aim of solving the problem of protein expression, methylotrophic yeasts such as *Hansenula polymorpha* and *Pichia pastoris* expression systems have been introduced.

Pichia pastoris is a methylotrophic yeast, capable of metabolizing methanol as its sole carbon source. The first step in the metabolism of methanol is the oxidation of methanol to formaldehyde using molecular oxygen by the enzyme alcohol oxidase (AOX). In addition to formaldehyde, this reaction generates hydrogen peroxide and to avoid hydrogen peroxide toxicity, methanol metabolism takes place within a peroxisome, which eliminates toxic byproducts away from the rest of the cell (Cereghino and Cregg, 2000) (Figure 6).

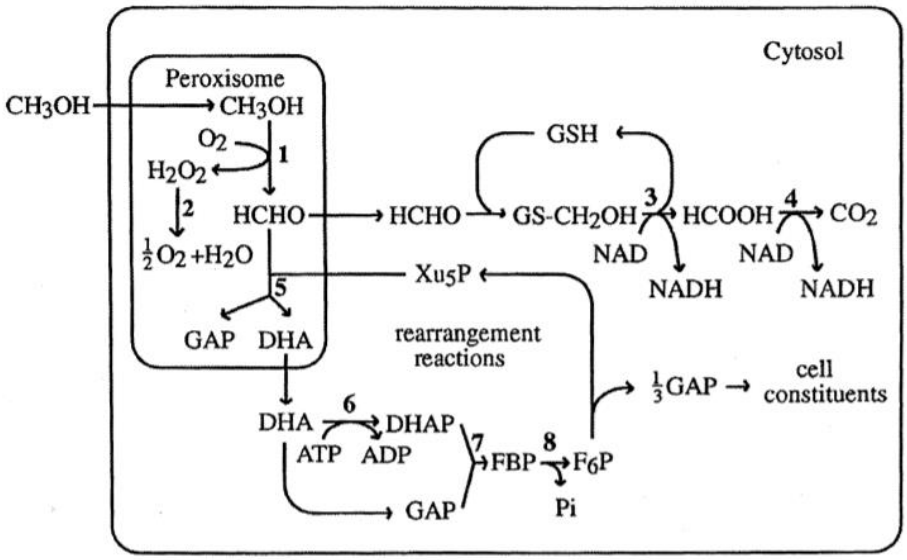

Figure 6. The methanol pathway in *P. pastoris* (adapted from Careghino and Cregg, 2000)
1, alcohol oxidase; 2, catalase;
3, formaldehyde dehydrogenase;
4, formate dehydrogenase;
5, dihydroxyacetone synthase;
6, dihydroxyacetone kinase;
7, fructose 1,6-biphosphate aldolase;
8, fructose 1,6-bisphosphatase

The promoter regulating the production of alcohol oxidase is the one used to drive heterologous protein expression in Pichia. Two genes in *Pichia pastoris* code for alcohol oxidase – AOX1 and AOX2. Expression of the AOX1 gene is tightly regulated and induced by methanol to very high levels, typically > 30 % of the total soluble protein in cells grown with methanol (Invitrogen, 2010). Although both genes are used to produce an alcohol oxidase, AOX1 produces more enzyme. Therefore, by knocking out the AOX1 gene, the growth on methanol is slowed down drastically with so called, methanol utilization slow (Mut^S) phenotype. A knockout of the AOX2 gene will not decelerate growth on methanol and the growth rates are comparable to methanol utilizing plus (Mut^+) phenotype (wild type). However, by knocking out both genes, the strains are unable to grow on methanol (methanol utilizing minus (Mut^-) (Cámara et al., 2017).

However, like other expression systems, this has some disadvantages. In the transformation stage, in comparison to the bacterial system, competent cells require large (µg-level) amounts of the plasmid, since the number of *E. coli* transformants is higher than *P. pastoris* transformants per µg of DNA (Wu and Letchworth, 2004). Furthermore, protein production in yeast systems is dependent on the consumption of methanol. Based on EasySelect™ Pichia Expression Kit (Invitrogen, Carlsbad, CA), at least 0.5 % concentration of methanol is required for the expression of recombinant proteins. The production could reach to the maximum level of 2–2.5 % (wt/vol) of methanol, but high levels of methanol concentrations (above 5 %) are very toxic for cell viability and can stop the production process (Santoso et al., 2012).

A wild-type *Pichia* strain X-33, useful for selection on Zeocin™ and large-scale growth, was used as an expression system in the experimental part of this thesis.

2.7. GOAL OF THE THESIS

Driven by latest research and with a lot of space for improvement, goal of this thesis was to produce and characterize different variants of *Myriococcum thermophilum* CDH with altered cofactor binding and kinetic stability. Mutations were introduced into the *Myriococcum thermophilum* CDH gene by site directed mutagenesis, expressed in X-33 *Pichia pastoris* cells. By mutations close to the FAD (G317 or G237) the FAD environment should be changed to alter kinetic stability. In comparison to *An*GOx and *Gc*GDH with higher oxygen turnover, mutations with substituted glycine were introduced. Secondly, the loop motif covering the FAD, also shows higher flexibility compared to *An*GOx and *Gc*GDH; simply because these loops are longer by ~10 amino acids, mutations should stabilize the loop by directly filling gaps and removing water (T305I, I294F) or by forming more stable salt bridges (D305E). For the loop mutations also the cytochrome domain might be affected; therefore, interdomain electron transfer might be altered. Figure 7 represents mutations introduced into *Mt*CDH (green), $FADH_2$ and the magenta colored cellobionolactone - an inhibitor of CDH, very similar to cellobiose.

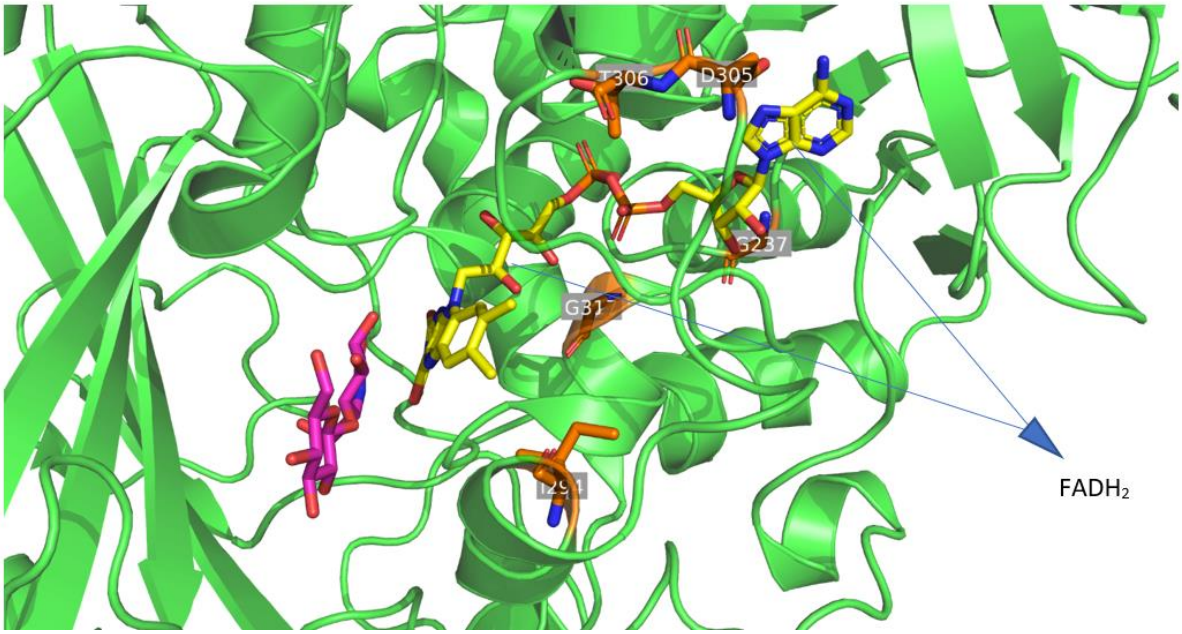

Figure 7. Mutations introduced into the *Mt*CDH

Visualization and modeling were performed by using PyMOL (Open Source PyMOL v2.3, Schrödinger, USA).

3. EXPERIMENTAL PART

3.1. CHEMICALS AND MEDIA

3.1.1. Chemicals

All chemicals used during this thesis were purchased from Sigma-Aldrich (St. Louis, Missouri, USA), Fluka (Vienna, Austria) or Carl Roth (Karlsruhe, Germany) and were of analytical grade or of highest purity available.

For the preparation of aqueous solutions reverse osmosis deionized water (RO-H_2O) or deionized and purified water (HQ-H_2O) by a Siemens Ultra Clear Basic UV SG system were used.

3.1.2. Media

All media used in *Pichia* expression were prepared according to the "Easy select *Pichia* Expression Kit manual" (Invitrogen, 2010). Zeocin was used as selection antibiotics and added to a final concentration of 25 mg L^{-1} for *E. coli* and 100 mg L^{-1} for *P. pastoris*.

***Escherichia coli*:**

- LB (Luria broth) + Zeocin) agar:

10 g L^{-1} NaCl
5 g L^{-1} Yeast Extract
10 g L^{-1} Peptone
15 g L^{-1} Agar-agar

The medium was autoclaved after dissolving and cooled to approximately 50 ºC after which pouring to sterile Petri dishes was carried out. For media with Zeocin, LS-LB (low salt-Luria broth) was prepared with 5 g L^{-1} NaCl and after sterilization and cooling down 25 mg L^{-1} Zeocin was added. For liquid medium, the preparation is the same, only without agar-agar.

- SOC (Super optimal broth with catabolite repression) medium (New England Biolabs, Ipswich, USA):

20 g L^{-1} Vegetable Peptone
5 g L^{-1} Yeast Extract
10 mM NaCl
2.5 mM KCl
10 mM $MgCl_2$
10 mM $MgSO_4$
20 mM Glucose

3.1.3. Media for *Pichia pastoris*

- Yeast Extract Peptone Dextrose (YPD) medium

20 g L^{-1} Peptone
10 g L^{-1} Yeast Extract
4 g L^{-1} Glucose
15 g L^{-1} Agar-Agar for Agar plates

<u>Deep well plate screening:</u>

- Buffered Yeast Peptone Dextrose (BYPD) Medium

20 g L^{-1} Peptone
10 g L^{-1} Yeast Extract
4 g L^{-1} Glucose
100 mM Potassium phosphate buffer (pH 6.0)

- Buffered Methanol-complex (BMMY) Medium

20 g L^{-1} Peptone
10 g L^{-1} Yeast Extract
100 mM Potassium Phosphate Buffer (pH 6.0)
100 mL L^{-1} YNB (10x)
2 mL L^{-1} Biotin (500x)
20 mL L^{-1} Methanol (100 %)

Expression of CDH in shaking flask cultures:

- Buffered Glycerol-complex (BMGY) Medium

20 g L^{-1} Peptone
10 g L^{-1} g L^{-1} Yeast Extract
100 mM Potassium Phosphate Buffer (pH 6.0)
100 mL L^{-1} YNB (10 ×)
2 mL L^{-1} Biotin (500 ×)
100 mL L^{-1} Glycerol (10 ×)

BMMY and BMGY media preparation (1 L):

10 g of yeast extract and 20 g of peptone were dissolved in 700 mL HQ-H_2O and autoclaved for 20 min on liquid cycle. After it was cooled to the room temperature, following was added and mixed well: 100 mL 1 M potassium phosphate buffer, pH 6.0, 100 mL 10 × YNB, 2 mM 500 × biotin and 100 mL 10 × glycerol. For BMMY 100 mL 10 × of methanol was added instead of glycerol. Media were stored in the 4 °C room.

3.1.4. Stock solutions

- **Yeast Nitrogen Base (YNB) (10 ×)**

34 g L^{-1} YNB without amino acids and ammonium sulphate
100 g L^{-1} Ammonium sulphate

YNB without amino acids and ammonium sulphate dissolved in HQ-H_2O using the sonicated water bath

- **Biotin (500 ×)**

200 mg L^{-1} Biotin

- **Glycerol (10 ×)**

100 mL L^{-1} Glycerol

- Basal Salts Medium (BSM)

26.7 mL L^{-1} Phosphoric acid (85 %)
1.18 g L^{-1} $Ca_2SO_4 \cdot 2\ H_2O$
18.2 g L^{-1} K_2SO_4
14.9 g L^{-1} $MgSO_4 \cdot 7\ H_2O$
4.13 g L^{-1} KOH
4.35 mL L^{-1} *Pichia* Trace Metals (PTM)
4 % (v/v) Glycerol
1 mL L^{-1} Antifoam 204

- Glycerol Feed Solution

50 % (v/v) Glycerol
12 mL L^{-1} *Pichia* Trace Metals (PTM)

- Methanol Feed Solution

100 % (v/v) Methanol
12 mL L^{-1} Pichia Trace Metals (PTM)

- *Pichia* Trace Metals (PTM)

2 g L^{-1} H_3BO_3
80 mg L^{-1} NaI
3 g L^{-1} $MnSO_4 \cdot H2O$
20 g L^{-1} $ZnCl_2$
0.2 g L^{-1} $Na_2MoO_4 \cdot 2\ H_2O$
6 g L^{-1} $CuSO_4 \cdot 5\ H_2O$
0.5 g L^{-1} $CoCl_2$
65 g L^{-1} $FeSO_4 \cdot 7\ H_2O$
0.2 g L^{-1} Biotin
5 mL L^{-1} Sulfuric acid

- 1 M Potassium phosphate buffer

132 mL K_2HPO_4 (1 M)
868 mL K_2HPO_4 (1 M)

If needed the pH was adjusted with KOH and phosphoric acid.

3.1.5. Other solutions

- DCIP solution

87.03 mg 2,6-dichloroindophenol (DCIP) were dissolved in 10 mL 96 % ethanol by stirring for 30 min at 50 °C. After complete dissolution, the solution was filled up to 100 mL with water. The solution was stored at 4 °C in the dark.

- Cytochrome *c* solution

12.4 mg cytochrome *c* were dissolved in 1 mL water. The solution was made directly before use and stored at 4 °C in the dark not longer than three days.

- 30 % glycerol

30 mL glycerol (≥ 99.0 %) was mixed with 70 mL water and sterilized by autoclaving 15 min at 121 °C. The solution was stored at 4 °C.

3.2. TRANSFORMATION AND SCREENING

Vector construction, site-directed mutagenesis, transformation of *E. coli* and electroporation of competent *Pichia pastoris* were performed by lab members.

3.2.1. Strains

- Bacteria

For the propagation of constructed plasmids NEB 5-alpha competent *Escherichia coli* (High Efficiency) cells were used. The cells were obtained from New England Biolabs (Ipswich, Massachusetts, USA).

- Yeast

For the production of *Mt*CDH variants, *Pichia pastoris* X-33 strain was used with Mut^+ (Methanol utilization plus) phenotype. Mut^+ refers to the wild type's ability of strains to metabolize methanol as the sole carbon source. *Pichia pastoris* X-33 cells from Thermo Fischer Scientific were used as expression host.

3.2.2. Site-directed mutagensis

For generation of different *Mt*CDH variants and the expression in *Pichia pastoris*, site-directed mutagenesis was used to create point mutations in the cellobiose dehydrogenase (CDH) cDNA and to produce the protein in high amounts. CDH cDNA was mutated with mutagenesis primers (sequence with point mutation) (Table 1) and PCR or error prone PCR. The mutated cDNA and the pPICZ A vector were transformed into *E. coli* for proliferation. The isolated plasmid was linearized and transformed into the expression host *Pichia pastoris* that secreted the mutated CDH extracellularly.

Table 1. Primes used for site-directed mutagenesis. Mutations were performed with the NEBaseChanger tool: https://nebasechanger.neb.com/

Desired mutation	Primer Name	Primer sequence
G237A	*Mt*CDH_G237A_F	TGTTGTCGGAGCTGGTGCCGGAG
	*Mt*CDH_G237A_R	ATGTAATCGAAAGAAACTCCAGTTGG
G237S	*Mt*CDH_G237S_F	TGTTGTCGGATCTGGTGCCGGAG
	*Mt*CDH_G237S_R	ATGTAATCGAAAGAAACTCC
I294F	*Mt*CDH_I294F_F	TTGCAACCAATTTTGGGTGGACTC
	*Mt*CDH_I294F_R	AGACCTGGAACGTCGAAA
D305E	*Mt*CDH_D305E_F	CGCTTGCGAGGAAACTGACCAAA
	*Mt*CDH_D305_R	ATTCCCTTAGAGTCCACCC
D305A	*Mt*CDH_D305A_F	CGCTTGCGAGGCTACTGACCAAA
	*Mt*CDH_D305_R	ATTCCCTTAGAGTCCACCC
T306I	*Mt*CDH_T306I_F	TTGCGAGGATATTGACCAAATGG
	*Mt*CDH_T306I_R	GCGATTCCCTTAGAGTCC
A310V	*Mt*CDH_A310V_F	TGACCAAATGGTTGGATGTGTTCTTGG
	*Mt*CDH_A310V_R	GTATCCTCGCAAGCGATTC
G317A	*Mt*CDH_G317A_F	TCTTGGTGGAGCTACCGCAGTCA
	*Mt*CDH_G317_R	ACACATCCTGCCATTTGG
G317S	*Mt*CDH_G317S_F	TCTTGGTGGATCTACCGCAGTCAATGC
	*Mt*CDH_G317_R	ACACATCCTGCCATTTGG

3.2.3. Vector construct

For the expression in *Pichia pastoris* and the proliferation of plasmids in *E. coli* the vector pPICZ A (Invitrogen, Carlsbad, California, USA), which is 3329 bp in length, was used (Figure 8). The regulation of the AOX1 gene is a two-step process: a repression/derepression mechanism and an induction mechanism. The BleoR gene expresses a protein which allows the binding of the antibiotic Zeocin (Invitrogen, Carlsbad, California, USA), which is used as a positive selection marker in *E. coli* and *P. pastoris*. The vector also contains an origin of replication (ori) that allows replication and maintenance of the plasmid in *E. coli*, and a promoter region, which enables the inserted genes to be transcribed into mRNA.

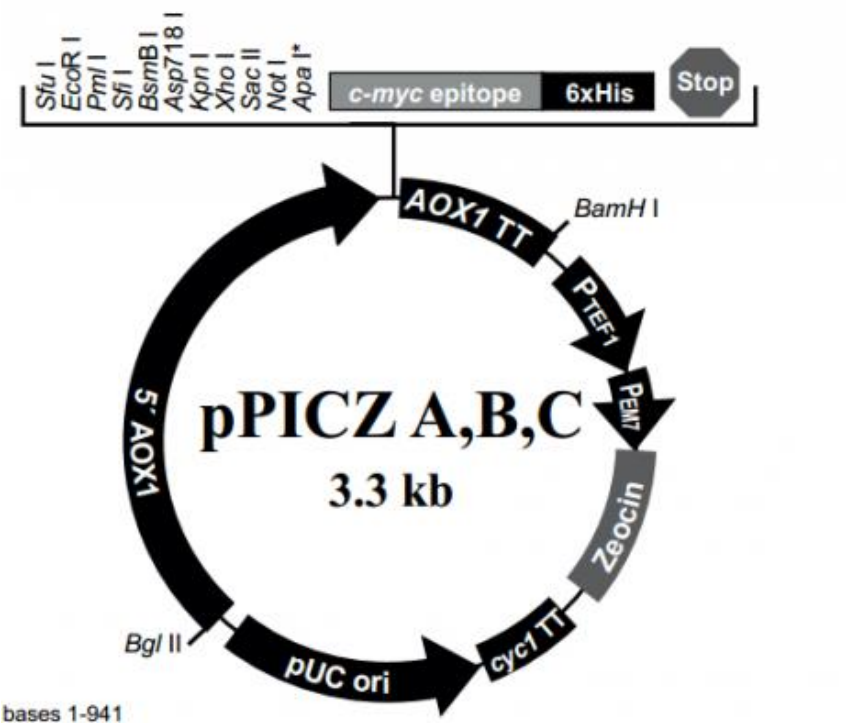

Figure 8. pPICZ vector used for the expression of *Mt*CDH variants (adapted from Life Science Market, 2021)

3.2.4. Chemical transformation of *E. coli* NEB 5-alpha cells

The PCR amplified and digested DNA was used for the transformation into chemically competent NEB5α cells according to the manufacturer's instructions. 50 µL of chemically competent *E. coli* NEB 5-alpha cells were thawed on ice and mixed with 1-5 µL DNA. After an incubation for 30 min on ice, the suspension was heat-shocked at 42 °C for 30 s and immediately placed back on the ice for 2 min. 950 µL of room temperature SOC media was

added, and the suspension was incubated for one hour at 37 °C and 250 rpm. The transformed cells were plated on LB plates supplemented with 25 mg L^{-1} Zeocin and incubated at 37 °C. Colonies from the transformation plates were picked, inoculated into 3 mL LB medium containing 25 mg L^{-1} Zeocin and incubated at 37 °C.

3.2.5. Plasmid isolation

Plasmid isolation was performed with the Monarch® Plasmid Miniprep Kit (New England Biolabs, Ipswich, Massachusetts, USA). To isolate the cloned plasmids, five single colonies of *E. coli* cells plated on the selective media were picked with a sterile toothpick and transferred to individual vials containing 3 mL LB + Ampicillin broth. The vials were incubated 37 °C and 180 rpm overnight. 1.5 mL of cell suspension was pipetted into an Eppendorf tube and centrifuged for 1 min at 16 000 × g. The supernatant was discarded, and the pellet resuspended in 200 µL plasmid resuspension buffer. The lysis of bacterial cells was achieved by adding plasmid lysis buffer, after which the tube was gently inverted five times until the color of the solution turned dark pink. After a brief incubation period of one minute, 400 µL of cold plasmid neutralization buffer were added and the tube was inverted until the color turned yellow. The solution was incubated for 2 min after which the lysate was clarified by centrifuging the tube for 3 min at 16 000 × g. The resulting supernatant was transferred to a spin column and spun down for 1 min. The flow-through was discarded and 200 µL of plasmid wash Buffer 1 added. The solution was incubated for 5 min before centrifuging for one min and discarding the flow-through. 400 µL of plasmid wash Buffer 2 were added and the solution was centrifuged for 1 min. The column was inserted into a clean 1.5 mL Eppendorf tube, 40 µL of sterile 50 °C HQ-H_2O was added and the tube was spun down for 1 min at 16 000 × g after two min of incubation. The solution was stored at -20 °C. Correct insertion of the genes and absence of mutations were confirmed by DNA sequencing (Microsynth AG).

3.2.6. Preparation of electrocompetent *Pichia pastoris* X-33 (Mut^+)

For the preparation of electrocompetent *P. pastoris* X-33 cells, frozen culture collections (-80 °C) of *P. pastoris* X-33 and from Invitrogen were used. For the precultures, 2 × 50 mL YPD medium in 250 mL baffled shaking flasks were inoculated with a freshly grown single colony. The precultures were inoculated overnight at 30 °C and 130 rpm. The precultures were then used to inoculate 2 × 250 mL YPD medium in 1-L baffled shaking flasks to a final OD_{600} of 0.15. The main cultures were incubated at 30 °C and 130 rpm. When the cells reached an OD_{600} of around 1 (after approx. 6 h), the cells were divided into two parts and harvested by

centrifugation at 4000 rpm and 4 °C for 10 min each. The cell pellets were resuspended in 50 mL YPD medium and 1 mL HEPES buffer (pH 8.0) each. While gentle shaking, 1.25 mL of a 1 M dithiothreitol (DTT) was added to each culture and incubated for 15 min at 30 °C, gently shaking with 100 rpm. Then, the volume of each culture was brought to 200 mL with sterile and cold HQ-H_2O and centrifuged (3000 rpm, 4 °C, 5 min). During the following steps the cell cultures were kept on ice all the time. After discarding the supernatant, the pellets were resuspended in 200 mL sterile and cold HQ-H_2O and centrifuged again (3000 rpm, 4 °C, 5 min). This washing step was repeated once. After washing the pellet, it was resuspended in 10 mL sterile and ice-cold 1 M sorbitol and pelleted again with 4000 rpm and 4 °C for 10 min. The supernatant was discarded, and the remaining pellet was resuspended in 0.5 mL ice-cold 1 M sorbitol and divided into 50 µL aliquots. The aliquots were frozen at -80 °C.

3.2.7. Electroporation of electrocompetent *Pichia pastoris* X-33 (Mut^+)

Prior to electroporation, the plasmids were linearized with PmeI, obtained from New England Biolabs (Ipswich, Massachusetts, USA) to support the integration into the 5´-AOX1 region in the *P. pastoris* genome. 4 µL of the digested plasmid (40 ng μL^{-1}) were added to 50 µL electrocompetent cells. The mixture was added to a pre-cooled, sterile 1 mm electroporation cuvette. Electroporation was carried out at 1.5 kV and 3 msec (manual settings in the MicroPulser electroporation system from Bio-Rad). After electroporation, the cells were immediately resuspended in 500 µL ice-cold, sterile 1 M sorbitol and 500 µL YPD medium. The suspension was transferred into a 2 mL tube and incubated at 30 °C with horizontal shaking at 90 rpm for 3 to 4 h. 100 µL of the cells were plated on YPD plates containing 100 mg L^{-1} Zeocin.

3.2.8. Cryo-culture

A single *Pichia pastoris* colony was cultivated in YPD medium at 30 °C for 24 h. 750 µL cell culture was mixed with 750 µL sterile glycerol (30 %) and frozen and stored at -80 °C

3.2.9. CDH deep well plate screening

This method was applied for the fast screening of enzymes variants produced in *P. pastoris* X-33. The cells expressing the enzyme variants under the control of the inducible *AOX* promoter were cultivated in deep well plates and the secreted protein was harvested in the supernatant and further analyzed for the properties of interest.

Pichia pastoris variants expressing the proteins of interest are transferred to YPD + Zeocin plate and incubated at 30 °C for 40 h. For each protein of interest six colonies of transformed *Pichia pastoris* cells were chosen from YPD + Zeocin selective plates. 250 µL of the BYPD medium was transferred to selected wells and inoculated with a single colony from the YPD + Zeocin plate. The 96-well plate was sealed with Breathe-Easy sealing membrane (Sigma-Aldrich, St. Louis, Missouri, USA) and incubated for 65 h at 30 °C and 300 rpm. After 65 h of incubation, the protein expression was induced by adding 250 µL of BMMY medium. 50 µL of methanol feed medium was added after further 8, 24 and 48 h. The cultivation was stopped after 136 hours, and cells were pelleted at 3500 rpm for 15 min in the centrifuge. The supernatant containing the enzyme was used for the screening procedure.

The activity of *Mt*CDH variants was determined by the cytochrome c activity assay and the cells from colonies that gave the highest specific activity of expressed protein were used for the production in shaking flasks.

3.3. ENZYME PRODUCTION

After the screening procedure, the most promising producers were chosen to produce enzymes of interest. Altogether there were five productions in shaking flasks – G317S *Mt*CDH, G317A *Mt*CDH, G237S *Mt*CDH, T306I *Mt*CDH and D305A *Mt*CDH in *Pichia pastoris* X-33 and G317S *Mt*CDH in *Pichia pastoris* X-33 in the BioFlo bioreactor. The procedure for the expression was based on the ″EasySelect *Pichia* Expression Kit″ by Invitrogen (2010).

3.3.1. Protein expression in baffled flasks

Pichia pastoris cells from a cryo-culture were transferred using a sterile toothpick to YPD + Zeocin agar plates and incubated at 30 °C for 48 hours. For the preparation of a preculture, 20 mL of YPD with 100 mg L^{-1} of Zeocin was inoculated with single colony from screening agar plate in a 100 mL baffled shaking flasks overnight at 30 °C and 130 rpm. 20 mL of preculture was used to inoculate 200 mL of BMGY medium in 1-L baffled flasks. Five flasks were used for expression of each of variants. Methanol was used for the induction, and it was added twice a day – to the concentration of 0.5 % in the morning and 0.8 % in the evening. The flasks were covered with two layers of sterile gauze for better oxygen dissolution. Samples were taken twice a day to measure optical density (OD_{600}) and analyze expression levels after methanol induction. Samples were centrifugated and the supernatants were analyzed for activity assays. In addition, protein concentration of harvested supernatant was determined using the Bradford assay.

3.3.2. Protein expression in the BioFlo bioreactor

Production of G317S *Mt*CDH in *Pichia pastoris* X-33 was performed in a 5-L BioFlo fermenter with the Eppendorf BioFlo120 fermentation system as control station (Figure 9). For the pre-precultures, 3 × 50 mL BMGY supplemented with 100 mg L^{-1} Zeocin were inoculated with a single colony freshly grown on a YPD plate. The colonies were incubated at 30 °C and 120 rpm. After 21 h, the cultures were diluted with BMGY medium to a final OD_{600} of 0.2 and a final volume of 160 mL, respectively. The three precultures were again incubated at 30 °C and 120 rpm for another 21 h. Two of the three cultures were used for inoculating the bioreactor. Before inoculation, the bioreactor was prepared by putting 3.2 L basal salts medium (BSM) to a 5-L heat-blanketed, autoclavable glass vessel. After autoclaving, the pH was set to 5.0 with 25 % NH_4OH and maintained for the entire fermentation process. The cultivation temperature was kept at 30 °C during the whole fermentation process. The stirrer speed was initially set to 700 rpm and increased to 900 rpm after the glycerol fed batch was started. The air flow rate

was set to 1 vvm (gas volume flow per unit of liquid volume per min) throughout the process. The fermentation was performed according to the *Pichia* Fermentation Guideline of Invitrogen with minor alterations (Invitrogen, 2010). After depletion of glycerol, the glycerol fed batch was initiated with a 50 % w/v glycerol feed medium containing 12 mL L^{-1} PTM trace salts to further increase biomass. The feed rate was adjusted to keep the DO level at 20 %. Recombinant protein production was induced by adding 18.8 mL of 100 % methanol (0.5 % v/v). After a transition phase of 4 h, a pulsed feed program was started, and every 1.5 h 16 mL of methanol feed (containing 12 mL L^{-1} PTM) were automatically added by the program. After a total cultivation time of 50 h this interval was reduced, and 16 mL methanol feed were added every 1.25 h. After a total cultivation time of 120 h (94 h on methanol) the fermentation was stopped to avoid proteolytic digestion and autolysis of the enzyme.

Figure 9. 5-L BioFlo fermenter with the Eppendorf BioFlo120 fermentation system as control process control system

3.4. ENZYME PURIFICATION

3.4.1. Cell removal and ammonium sulfate addition

The cells were removed from the fermentation broth by a centrifugation at 8500 rpm for 40 min at 4 °C and the supernatant was collected and filtered. Then, 100 % saturated ammonium sulfate solution was slowly added to the cooled supernatant to 30 % saturation. The clear supernatants containing the enzyme was purified using two chromatographic steps – hydrophobic affinity chromatography (HIC) and anion exchange chromatography (AEX).

3.4.2. Hydrophobic interaction chromatography (HIC)

The first purification step (HIC) was performed on a Phenyl Sepharose FF (fast flow) column (220 mL) using an Äkta Explorer system (GE Healthcare Bio-Sciences, Pittsburgh, Pennsylvania, USA) (Figure 10).

Figure 10. Äkta Explorer system with Phenyl Sepharose Fast Flow column

After the column was equilibrated with HIC Buffer A (25 mM sodium acetate, pH 5.5, 30 % ammonium sulphate), the supernatant containing 30 % ammonium sulphate was loaded onto the column. This is due to partial unfolding of the protein which allows hydrophobic groups to surface and bind to the hydrophobic stationary phase. After loading the supernatant, the column was washed with buffer A until all unbound protein was eluted from the column and the conductivity reading was constant. Elution was performed over a linear gradient of 3 column volumes (CV) from 0 to 100 % Buffer B at a flow rate of 12 mL min^{-1} and collected in 10 mL fractions. The pooled enzyme-containing fractions were ultrafiltrated using Amicon Ultra-30 Centrifugal Filters (Millipore, Burlington, Massachusetts, USA) with a molecular

weight cut-off (MWCO) of 30 kDa. A buffer exchange to 10 mM HEPES, pH 7.0 was performed until the conductivity was below 3 mS cm^{-1}. During all chromatography steps absorbance at 280 nm (aromatic amino acids), 420 nm (heme *b*) and 450 nm (FAD) as well as conductivity values were monitored online. Conditions and specifications shown in Table 2 were used for the first step of enzyme purification.

Table 2. Hydrophobic interaction chromatography conditions and specifications

Column material	**Phenyl Sepharose Fast Flow (GE Healthcare, USA)**
Column volume	220 mL
Buffer A (loading buffer)	25mM sodium-acetate buffer, pH 5.5 + 30 % ammonium sulfate saturation
Buffer B (elution buffer)	25 mM sodium-acetate buffer, pH 5.5
Flowrate	10-15 mL min^{-1}
Gradient	0-100 % buffer B (linear gradient in 3 CV)

3.4.3. Anion exchange chromatography (AEX)

The second purification step was anion exchange chromatography and was performed using an Äkta Pure system (GE Healthcare Bio-Sciences, Pittsburgh, Pennsylvania, USA) (Figure 11).

Figure 11. Äkta Puresystem with Q Source 30 column

The rebuffered enzyme solution was applied to a Source 30 Q resin (52 mL column volume) equilibrated with 10 mM HEPES buffer, pH 7.0. Proteins were eluted in a linear gradient over 5 CV from 0 to 50% Buffer B at a flow rate of 10 mL min^{-1} . The proteins were collected in 10 mL fractions and pooled according to activity, SDS-PAGE and highest 420/280 nm ratio (RZ number, see 3.5.2.4.). The pooled fractions were concentrated and a buffer exchange to 20 mM HEPES, pH 7.0 was again performed with Amicon Ultra-30 Centrifugal Filters (Millipore, Burlington, Massachusetts, USA) with a molecular weight cut-off (MWCO) of 30 kDa. Conditions and specifications shown in Table 3 were used for the second step of enzyme purification.

Table 3. Anion exchange chromatography conditions and specifications

Column material	**Q Source 30** **(GE Healthcare, USA)**
Column volume	52 mL
Buffer A (loading buffer)	10 mM HEPES, pH 7.0
Buffer B (elution buffer)	10 mM HEPES, pH 7.0 + 1 M NaCl
Flowrate	10-15 mL min^{-1}
Gradient	0-50 % Buffer B (linear gradient in 10 CV)

3.4.4. Centrifugal ultrafiltration

For concentrating of the protein solution to the target concentration for i.e., stopped-flow or thermofluor measurements, Amicon Ultra-2 Centrifugal Filters for DNA and Protein Purification and Concentration (Millipore, Burlington, Massachusetts, USA) with a molecular weight cut-off (MWCO) of 10 kDa were used. The solution to be concentrated was loaded into the ultrafiltration device and centrifuged at 4000 × g. The flow-through was discarded and the procedure repeated until the protein solution was concentrated to the desired concentration.

3.5. PROTEIN CHARACTERIZATION AND QUALIFICATION

3.5.1. Wet biomass determination

Wet biomass was determined for samples taken during shaking flask expression and protein expression in the bioreactor. Therefore, 1 mL of the culture taken aseptically were put to 1.5 mL tubes, of which the tara weight has been determined in advance and centrifuged 5

min at 13000 rpm. After centrifugation, the supernatant was removed and used for protein concentration and enzyme activity determination. The weight of the reaction tube containing the cell pellet was determined and wet biomass calculated by subtracting the weight of the full tube by the weight of the empty tube. Wet biomass was determined in triplicates for each sample.

3.5.2. Protein concentration

To monitor the cultivation process and the course of the purification the protein concentration was determined using the rapid protein quantification method developed by Bradford (1976).

The protein concentration of the purified homogenous protein solutions was determined spectrophotometrically at 280 nm using a molar absorption coefficient calculated from the amino acid sequence of the protein.

3.5.2.1. Bradford assay

Determination of the total protein concentration was done with the Bradford assay. Therefore, 980 µL Bradford reagent and 20 µL sample were incubated for 15 min at room temperature and the absorbance of the mixture was determined spectrophotometrically at 595 nm with a Beckman Coulter DU 800 UV/VIS spectrophotometer (Beckman Coulter, Brea, California, USA). The protein concentration was calculated using a calibration curve of bovine serum albumin in the range of 0.1 – 1.0 mg mL^{-1}. Bradford stock reagent and bovine serum albumin standards were purchased from Bio-Rad Laboratories (Hercules, California, USA) and prepared according to the manufacturer´s instructions.

3.5.2.2. Spectrophotometry

Homogeneous enzyme concentration was determined in a 1 cm quartz cuvette, from the absorption at 280 nm, using the calculated molar extinction coefficient for target protein. To convert between absorption and protein concentration Lambert-Beer law was used:

$$A = \varepsilon \cdot c \cdot l \qquad [5]$$

A … absorption

ε … molar absorption coefficient [M^{-1} cm^{-1}]

c … molar concentration [M]

l … pathlength [cm]

3.5.2.3. UV-Vis spectroscopy

To record the absorption spectra of pure enzyme solutions Agilent 8453 UV-visible Spectroscopy System (Agilent Technologies, California, USA) was used. The whole spectrum from 200 nm to 900 nm was recorded against a blank (buffer). The whole spectrum from 200 nm to 900 nm was recorded against a blank (buffer). The samples were diluted with the buffer used in the blank to not exceed an A_{280} of 1.5. Cytochrome concentrations were measured according to absorption at 420 nm.

3.5.2.4. Index of purity (RZ value)

Abbreviation RZ comes from a German word “Reinheitszahl“ which in German means purity number. To determine purity of CDHs, the RZ number was introduced as a 420 nm/280 nm ration of two peaks in the spectrum. For the *Trichoderma reesei* CDH there has already been shown that at highest purity ratio is 0.61 (Ma and Ludwig, 2019).

3.5.3. Enzyme activity assays

3.5.3.1. DCIP assay

This method is used as a standard method to determine CDH activity in crude extracts or purified preparations. DCIP (2,6-dichloroindophenol) is a redox indicator, which oxidized form is blue and changes to colorless during reduction. The reduction is independent from CYT and takes two electrons directly from the FAD. Therefore, it is a useful assay to determine the expression level of CDH and to standardize the results obtained from the other assays.

The measurements were performed using the Perkin Elmer Lambda 35 UV-VIS Spectrometer photometer (Waltham, Massachusetts, USA). All the solutions except the sample were pipetted in a cuvette and the mixture was incubated at 30 °C in a water bath for a minimum of 20 min and then transferred to the sample holder. The reaction begins when 20 µL of the sample was added to the cuvette, which was already placed in the sample holder. The result is a linear decrease of the absorbance at 520 nm recorded over 180 s. The pipetting scheme is presented below (Table 4).

Table 4. Pippeting scheme for DCIP assay

Solution	Concentration	Volume
DCIP solution (in 10 % (v/v) ethanol	3 mM	100 µL
Cellobiose solution	100 mM	100 µL
Sodium-acetate buffer pH 4.5	100 mM	780 µL
Enzyme solution		20 µL
Total volume in the cuvette		1000 µL

3.5.3.2. Cytochrome c assay

Cytochrome *c* (from bovine heart) is an efficient acceptor of only one electron, and it can solely be reduced at CYT. Thus, it serves as an indicator for improved or reduced IET properties of CDH. The activity of produced enzymes towards cytochrome *c* depends on the heme *b*-containing domain, whereas no reaction is observed if only the catalytic dehydrogenase domain, containing FAD as a cofactor, is present. The reaction was followed for 180 s at 30 °C and recorded at 550 nm. During the reduction cyt *c* changes its color from reddish to pink. The measurements were performed using the Perkin Elmer Lambda 35 UV-VIS Spectrometer photometer (Waltham, Massachusetts, USA). Cytochrome *c* solution, substrate solution and sodium-acetate buffer were pipetted in a cuvette and the mixture was incubated at 30 °C in a water bath for a minimum of 20 min and then transferred to the sample holder. The reaction started when 20 µL of the sample was added to the solution. Volumetric activity was automatically calculated by the software from the positive slope (increase) of the absorption The pipetting scheme is shown in Table 5.

Table 5. Pippeting scheme for cyt *c* assay

Solution	Concentration	Volume
Cytochrome *c* (in distilled water)	3 mM	20 µL
Cellobiose solution	100 mM	100 µL
Sodium-acetate buffer pH 4.5	100 mM	860 µL
Enzyme solution		20 µL
Total volume in the cuvette		1000 µL

3.5.4. pH-profile

A series of McIlvaine buffers was made with pH values ranging from 2.5 to 7.5 (steps of 0.5) by mixing 100 mM citric acid with 200 mM Na_2HPO_4 (Table 6). The activity at each pH value was measured as described before for the DCIP activity assay, the only difference being that the buffer used was not Na-acetate but the series of prepared buffers. Cellobiose (100 mM) was used as a substrate. The measurements were performed in triplicates using the Perkin Elmer Lambda 35 UV-VIS Spectrometer photometer (Waltham, Massachusetts, USA).

Table 6. Pipetting protocol for McIlvaine buffer preparation

McIlvaine buffer				
pH measured	pH	citrate 100 mM [mL]	Na_2HPO_4 200 mM [mL]	Total [mL]
	3	24.94	5.06	30
	3.5	20.91	9.09	30
	4	18.42	11.58	30
	4.5	16.38	13.62	30
	5	14.55	15.45	30
	5.5	12.93	17.07	30
	6	11.04	18.96	30
	6.5	8.70	21.30	30
	7	5.28	24.72	30
	7.5	2.37	27.63	30
	8	0.82	29.18	30
Total [mL]		136.34	193.66	330
Total + 10 % [mL]		**150**	**213**	
Weight [g]		**2.8813**	**7.5833**	
M [g mol^{-1}]		192.12	177.99	

3.5.5. Thermal stability

The thermal stability was determined by measuring the change of activity caused by a temperature gradient over 15 min (Table 7). CDH samples were diluted to a final volume of 70 µL for each temperature to measure triplicates and incubated in a MyLQ Single Color Real-Time PCR Detection System (BioRad, US). Volumetric activity was determined afterwards with cytochrome *c* activity assay following pipetting protocol in Table 5.

Table 7. Temperature profile: Temperature gradient stability properties

Time (min)	Temperature (°C)
	RT (22 °C)
	37
	40
	45
15	50
	55
	60
	65

3.5.6. Differential scanning fluorimetry (DSF)

A thermal shift assay (TSA) measures changes in the thermal denaturation temperature and stability of a protein under varying conditions such as variations in buffer pH, ionic strength or sequence mutation. The most common method for measuring protein thermal shifts is differential scanning fluorimetry (DSF) or thermofluor, which utilizes specialized fluorogenic dyes (Dart et al., 2018).

The thermal stability of a given protein is typically described by the thermal unfolding transition midpoint temperature T_m (°C), at which half of the protein population is unfolded. T_m is calculated from the changes in tryptophan fluorescence intensity, or from the ratio of tryptophan emission at 330 and 350 nm, which describes the shift of tryptophan emission upon unfolding. Typically, the 350/330nm ratio yields data with well-defined transitions upon protein unfolding, whereas the single wavelength detection does not always allow one to derive the T_m.

Thermodynamic stability was measured by an advanced Differential Scanning Fluorimetry technology (nanoDSF) using a capillary-based instrument Prometheus NT.48 instrument (NanoTemper Technologies, US) (Figure 12) and analyzed with the PR.Thermocontrol v.2.15 Software. Cellobiose dehydrogenase concentrations were adjusted to 2.0 mg mL^{-1} based on their molar extinction coefficients at 280 nm. All measurements were carried out in McIlvaine buffer, pH from 3 to 8, with a linear temperature gradient from 20 to

95 °C at a scan rate of 1.0 °C min^{-1}. Transition midpoint temperatures (T_m) of the enzymes were determined from the peak maximum of transition (NanoTemper Technologies, 2015).

Figure 12. Prometheus NT.48 instrument + High Sensitivity Capillaries for sampling

3.5.7. Steady-state kinetic studies

Steady-state kinetics can be described by the Michaelis-Menten equation, which states the quantitative relationship between the velocity v_0, the maximum velocity V_{max} ant the initial substrate concentration [S], all related through the Michaelis-Menten constant K_M. It applies whenever the concentration of the substrate is well above that of the enzyme, so that the rate of change of substrate concentration greatly exceeds the rate of change of the concentration of any enzyme form (Sassa et al., 2013).

The kinetic constants K_M, k_{cat} and V_{max} were determined for cellobiose as a natural substrate in 100 mM sodium-acetate buffer pH 4.5. The change in activity was monitored using DCIP activity assay over 180 sec at 30 °C. K_M and V_{max} values were calculated using the online tool https://mycurvefit.com/. Knowing these parameters, the turnover number k_{cat} and the catalytic efficiency (k_{cat}/K_M) were calculated by using the molecular mass of CDH.

The initial substrate concentrations used to measure enzyme activity were:

- cellobiose: 5.6, 11.1, 22.2, 44.4, 133.3, 400.0, and 1200 µM

The pipetting scheme for substrate stock solution preparation is shown in Table 8.

Table 8. Substrate stock solution preparation

Final (µM)	Stock (µM)	Stock (mM)	Dilutions to make stock conc. 1:	Volume stock (µL)	Volume water (µL)
5.6	55.6	0.06	2 1:2 from the 11.1 stock	1500	1500
11.1	111.1	0.11	2 1:2 from the 22.2 stock	1500	1500
22.2	222.2	0.22	2 1:2 from the 44.4 stock	1500	1500
44.4	444.4	0.44	3 1:3 from the 133.3 stock	1500	3000
133.3	1333.3	1.3	3 1:3 from the 400 stock	1500	3000
400	4000.0	4.0	3 1:3 from the 1200 stock	1500	3000
1200	12000.0	12.0	3 1:3 from the 3600 stock	1500	3000
3600	36000.0	36.0	Cellobiose stock	4500	

3.5.8. Presteady-state kinetic studies

With the stopped-flow technique it is possible to examine the presteady-state kinetics of fast, liquid-phase biochemical reactions by the rapid mixing of the reactants. Presteady-state measurements were carried out in a stopped-flow spectrophotometer (Applied Photophysics SX 20, Leatherhead, UK) at 30 °C. A photodiode array detector (PDA; Applied Photophysics), which allows observation of absorbance at multiple wavelengths in the wavelength range 180 – 750 nm, was employed to monitor the rapid spectral changes at the isosbestic points of the FAD (449 nm) and the heme cofactor. The hemeprotein has two absorbing bands in the 500 – 600 nm region (Figure 13) at 533 nm (heme β-band) and 563 nm (heme α-band) with the α-band being chosen due to its higher absorption difference.

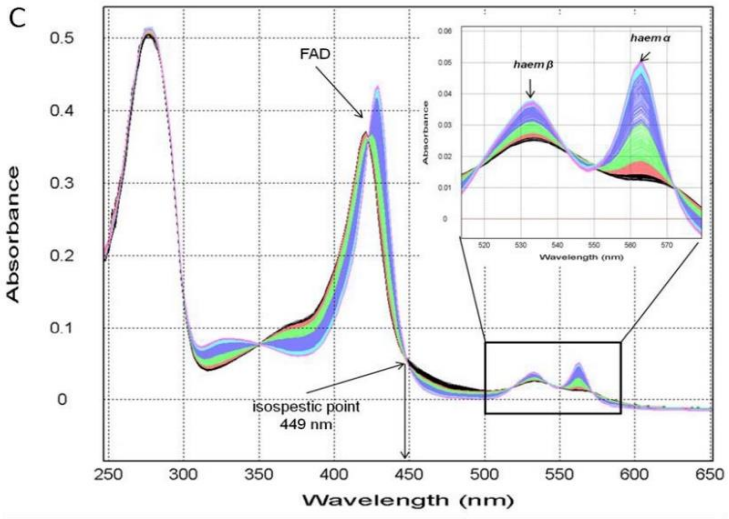

Figure 13. Presteady-state spectral changes of CDH upon mixing with cellobiose (Scheiblbrandner, 2012)

In order to determine the intra-electron transfer (IET) rates in between the DH and the CYT domains the presteady-state reduction of the heme was monitored by the SX-20 spectrophotometer applying a single mixing mode. Therefore, 5.5 μM CDH (final concentration) and an excess of cellobiose (50 μM final concentration) in 100 mM sodium-acetate pH 6.0, were pushed into an optical cell where the spectral data were collected by a photodiode array detection system, which was triggered after the flow has been stopped by a stop syringe. Absorption changes at 563 nm were used to monitor heme reduction and the observed rate (k_{obs}) was estimated by fitting the experimental data to a single exponential curve.

3.5.9. SDS-PAGE electrophoresis

Protein samples were diluted with 2 × Laemmli buffer (Thermo Fisher Scientific, Waltham, Massachusetts, USA), and incubated at 99 °C for 5 min. After spinning down the samples, 10-20 μL of each sample were loaded on a Mini-PROTEAN TGX precast gel with a gradient of 4-15 % polyacrylamide. 5 μL of the Precision Plus Protein Dual Color Standard (Bio-Rad Laboratories, Hercules, California, USA) were loaded on each gel for determining the molecular mass of the proteins under denaturing conditions. The gel was placed into an electrophoretic cell filled with 1 × running buffer and electrophoresis performed for approximately 60 min at 120 V. Proteins were visualized with the Gel Doc XRand Image Lab software (Bio-Rad, USA).

4. RESULTS AND DISCUSSION

The goal of this thesis was to produce and characterize different variants of *Myriococcum thermophilum* CDH. Altogether there were five productions in shaking flasks – G317S *Mt*CDH, G317A *Mt*CDH, G237S *Mt*CDH, T306I *Mt*CDH and D305A *Mt*CDH in *Pichia pastoris* X-33 and G317S *Mt*CDH in *Pichia pastoris* X-33 in the BioFlo bioreactor. The procedure for the expression was based on the ″EasySelect Pichia Expression Kit″ by Invitrogen (2010). Successfully produced enzymes were purified and characterized by thermal and kinetic stability assays.

All data is shown in the form of tables, figures, and pictures with a detailed explanation of their contents. After collection of all the data, it was analyzed and organized using the Microsoft Office 365 package (Microsoft, Redmond, Washington, USA) and SigmaPlot 12.0 (Systat Software, San Jose, California, USA).

4.1. DEEP WELL PLATE SCREENING

To confirm presence of two-domain enzyme in the supernatant and to select the best producers in 96-well plate, volumetric activity with cytochrome c as an electron acceptor was measured. Out of seven active enzymes, five (G317S, G317A, G237S, T306I and D305) were produced and fully characterized, as stated in Table 9. Because of mutation position, these were assumed to be the most promising and with great potential of improved thermal and kinetic stability.

Table 9. Overview of all CDHs examined during this work

Wild type	A310V	D305A	G237S	G317S	T306I	D305E	I294F	G317A
Volumetric activity detected								
+	-	+	+	+	+	+	+	+
Produced during this master thesis								
		+	+	+	+	-	-	+
Produced by other lab members								
+								
Characterized during this master thesis								
+		+	+	+	+	-	-	+

4.2. EXPRESSION IN SHAKING FLASKS AND ENZYME PURIFICATION

All the variants were recombinantly produced in *P. pastoris* X-33 under the control of the methanol inducible AOX promotor. The expression was performed in shaking flasks, except for G317S variant which was produced in shaking flasks and BioFlo Fermenter. After harvesting, two-step purification was proceeded and rebuffered and concentrated samples were frozen and stored.

4.2.1. G317S *Mt*CDH

4.2.1.1. Fermentation

After the preculture step (3.3.1.), protein expression of G317S *Mt*CDH was continued in five 1-L baffled flasks (Figure 15). After methanol induction, samples were taken twice a day to check volumetric activity using cytochrome *c* assay. The biomass was harvested after a total cultivation time of 95 h (73 h on methanol) by centrifugation. The culture reached OD_{600} of 24.8 with an external protein concentration of 0.22 g L^{-1} (determined with Bradford assay) and a volumetric DCIP activity of 0.018 U mL^{-1} and a volumetric cytochrome *c* activity of 0.0031 U mL^{-1} (Figure 14).

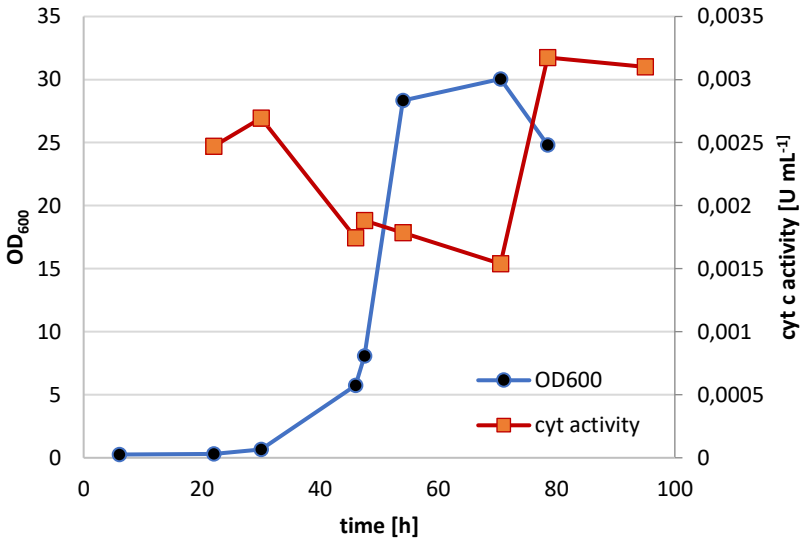

Figure 14. Production of the G317S *Mt*CDH in shaking flasks with curves for OD_{600} and cytochrome activity

Although the production of G317S *Mt*CDH was not very successful, which can be seen in the low volumetric enzyme activity and atypical OD_{600} curve, it was decided to purify the protein to gain more information about optimizing the upstream and downstream processes. Low yield in biomass (OD_{600}) could occur due to metal caps used during fermentation or too low rpm, thereby limiting the transfer of oxygen from the environment into the baffled flask. In addition, two of five flasks in the first fermentation were not baffled flasks which could also affect biomass growth. Instead of metal caps, cotton plugs were used for next fermentation. Furthermore, because of the low detected cytochrome activity, it was decided to use DCIP as an electron acceptor in activity assay for samples during fermentation. Lastly, instead of OD_{600}, wet biomass concentration (g mL^{-1}) was measured in next fermentations.

Figure 15. Production of *Mt*CDH in shaking flasks

4.2.1.2. Purification

After harvesting, ammonium sulphate was slowly added to the supernatant to a 30 % saturation (final). The recombinant enzyme was purified using a two-step purification protocol including HIC and AEX. The first step of purification was hydrophobic interaction chromatography in which the selected peak (absorption at 280 nm), was pooled manually. The protein peak appeared when Buffer B gradient reached 100 %. Pooled fraction and flow-through were separately analyzed by SDS-PAGE and spectrophotometrically. UV/VIS spectrum showed a characteristic absorbance peak at 420 nm for pooled fraction whereas the activity in flow-through was not detected. For pooled fraction, a buffer exchange to AEX Buffer A (25 mM potassium phosphate buffer, pH 7.0) was performed using Amicon Ultra-15 centrifugal filters with a cut-off of 30 kDa until the conductivity was below 3 mS cm^{-1}. After fraction loading, protein was eluted in a linear gradient from 0 to 50 % Buffer B and the only peak at 280 nm appeared at approximately 20 % Buffer B. Fraction was pooled manually and analyzed by SDS-PAGE and spectrophotometrically in which the UV/VIS spectrum showed an absorbance peak at 420 nm specific for heme *b* in samples (Figure 17). With the similar peak shape, manual pooling and only 280 nm detection wavelength, the chromatograms shown in Figure 16 apply to the G317A variant as well.

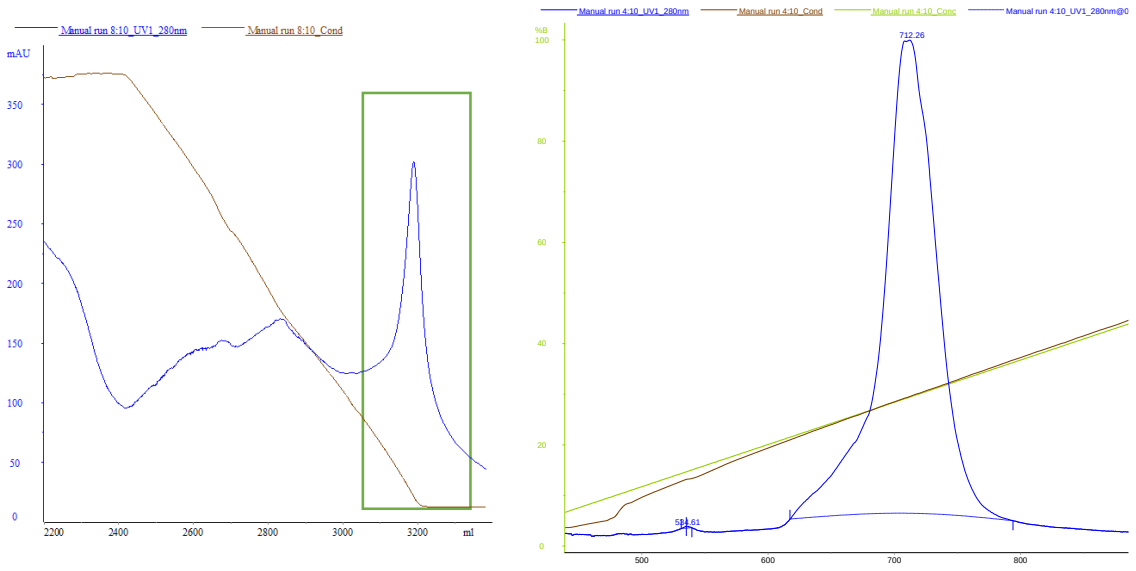

Figure 16. Purification chromatograms detected at 280nm during two-step purification: HIC (left) and AEX (right)

Table 10. Purification scheme for G317S *Mt*CDH and comparison within DCIP and cytochrome *c* assays, used for volumetric activity measurements

G317S	Vol. activity (DCIP)	Protein conc.	Spec. activity	Volume	Total activity	Total protein	Yield	Purification level
Step	U mL^{-1}	mg mL^{-1}	U mg^{-1}	mL	U	mg	%	
Supernatant	0.0176	0.223	0.0789	1040	18.304	231.92 *	100	1
HIC	0.0392	0.394	0.0995	200	7.840	78.78	42.8	1.26
AEX	0.581	1.876	0.3097	7	4.067	13.132	22.2	3.92
G317S	**Vol. activity (cyt *c*)**	**Protein conc.**	**Spec. activity**	**Volume**	**Total activity**	**Total protein**	**Yield**	**Purification level**
Step	U mL^{-1}	mg mL^{-1}	U mg^{-1}	mL	U	mg	%	
Supernatant	0.0031	0.223	0.0094	1040	2.184	231.92 *	100	1
HIC	0.0108	0.394	0.0274	200	2.160	78.78	98.9	2.91
AEX	0.1537	1.876	0.0819	7	1.076	13.13	49.3	8.70

*Supernatant concentration measured using Bradford assay

After each step, volumetric activities (DCIP and cytochrome *c* activity assays) and protein concentrations were detected. The protein concentration in Table 10 for HIC and AEX samples is determined in a 1 cm quartz cuvette, from the absorption at 280 nm, using the calculated molar absorption coefficient. With very low overall yield of the purification (22.2 %) as well as the final amount of purified enzyme, specific activity for purified enzyme is 0.3097 U mg^{-1}.

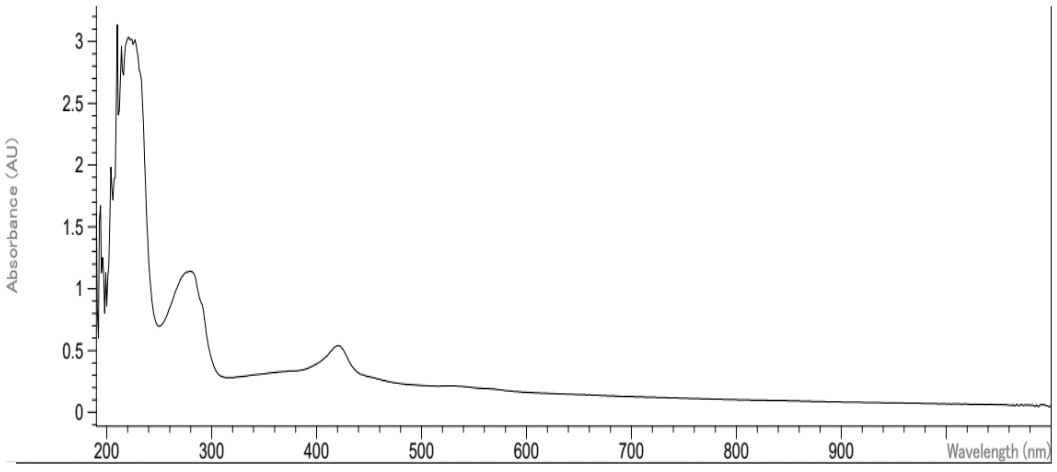

Figure 17. Spectrum of G317A *Mt*CDH purified enzyme with characteristic peaks at 280 nm and 420 nm

The A_{420}/A_{280} ratio (RZ number) for pure cellobiose dehydrogenase produced in different expression systems, including *Pichia pastoris*, is around 0.6 (Ma and Ludwig, 2019).

The RZ number for the purified G317S *Mt*CDH is 0.43, which divided by maximum 0.6 gives approximately 73.33 % purified enzyme. To confirm the purity a lane and band analysis by Imager ChemiDoc™ was performed and the purity of 76.3 % was recorded. Furthermore, Imager precisely calculates molecular weight of SDS-PAGE detected bands, and the size of target enzyme is 106.3 kDa (Figure 18). This result corresponds to the literature in which is stated that molecular mass ranges depend on the glycosylation, which can account for up to 20 % of the molecular mass (Ludwig et al., 2013). The 25-35kDa (size of CYT_{CDH} domain) difference in two obtained bands, could indicate that the 89.8 kDa protein is missing cytochrome domain because of insufficient heme *b* loading during protein expression (Hallberg et al., 2002). Other possibility is that the enzyme is not glycosylated, which is less likely for *Pichia pastoris* expression system.

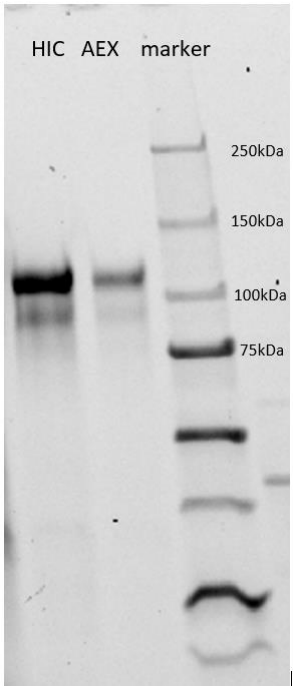

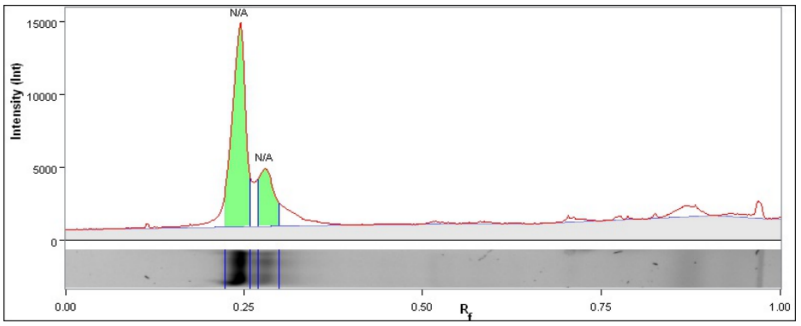

Band No.	Band Label	Mol. Wt. (KDa)	Relative Front	Volume (Int)	Abs. Quant.	Rel. Quant.	Band %
1		106,3	0,244	17 371 870	N/A	2,55	76,3
2		89,8	0,280	5 404 498	N/A	0,79	23,7

Figure 18. SDS-PAGE of HIC and AEX pooled fractions (left) and lane and band analysis by Imager ChemiDoc™ XRS+ 5.2.1. Imager Software for AEX band (right)

One of the commonly taken approaches to overcome deficient incorporation of heme in apo-proteins is supplementation of the growth medium with the desired cofactor. The yield of active recombinant heme peroxidase from *P. pastoris* can be enhanced by the addition of hemin, and therefore could be also considered for our target protein production (Krainer et al., 2015).

Instead of adding heme supplementation, to determine whether the problem is in pooling technique and insufficient amount of total protein in the supernatant, a fermentation in the 5-L

BioFlo fermenter, and a two-step purification using a fraction collector, was performed (see 4.3.).

4.2.3. G317A *Mt*CDH

As mentioned in 4.2.1., several modifications were implemented for next variant fermentation. Instead of metal caps, cotton plugs were used during this fermentation. Even though same rpm on the shaker was used, splashing of the medium was way too intense which resulted in soaked plugs. Initial volume of 1000 mL from the beginning dropped up to 697 mL (Table 11) and corresponding protein yield after harvesting could be lower due to the limited oxygen transfer in the medium during fermentation. However, fermentation data (Figure 19) for G317A show expected increasing trend for volumetric activity and biomass concentration, in contrast to G317S fermentation. The culture reached wet biomass concentration of 50.5 g L^{-1} with an external protein concentration of 0.251 g L^{-1} (determined with Bradford assay) and a volumetric DCIP activity of 0.0365 U mL^{-1} and a volumetric cytochrome c activity of 0.0106 U mL^{-1}.

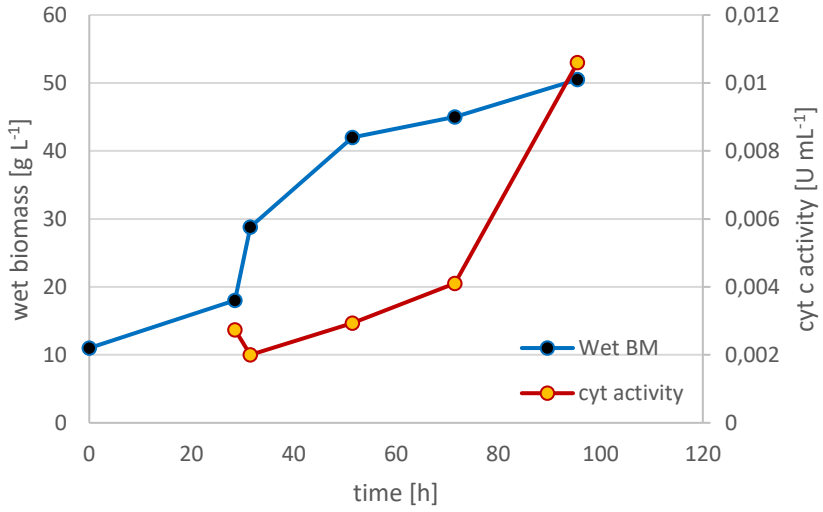

Figure 19. Production of the G317S *Mt*CDH in shaking flasks with curves for wet biomass concentration and cytochrome *c* activity

Two-step purification protocol is identical to the one used in G317S *Mt*CDH variant purification (see 4.2.2.). UV/VIS spectrum showed a characteristic absorbance peak at 420 nm for pooled HIC and AEX fraction whereas the activity in flow-through was not detected.

Table 11. Purification scheme for G317A *Mt*CDH and comparison within DCIP and cytochrome *c* assays, used for volumetric activity measurements

G317A	Vol. activity (DCIP)	Protein conc.	Spec. activity	Volume	Total activity	Total protein	Yield	Purification level
Step	U mL^{-1}	mg mL^{-1}	U mg^{-1}	mL	U	mg		
Supernatant	0.0365	0.251	0.1456	697	25.47	174.95	100	1
HIC	0.0563	0.342	0.1647	182	10.25	62.21	40.2	1.13
AEX	1.6010	6.210	0.2578	2.5	4.00	15.52	15.7	1.77

G317A	Vol. activity (cyt *c*)	Protein conc.	Spec. activity	Volume	Total activity	Total protein	Yield	Purification level
Step	U mL^{-1}	mg mL^{-1}	U mg^{-1}	mL	U	mg		
Supernatant	0.0106	0.251	0.0424	697	7.41	174.95	100	1
HIC	0.0316	0.342	0.0925	182	5.75	62.21	77.6	2.18
AEX	0.5203	6.210	0.0838	2.5	1.30	15.52	17.6	1.98

After each step, volumetric activities (DCIP and cytochrome *c* activity assays) and protein concentrations were detected. Protein concentration in Table 11 for HIC and AEX samples is determined in a 1 cm quartz cuvette, from the absorption at 280 nm, using the calculated molar extinction coefficient. With very low overall yield of the purification (15.72 %) as well as the final amount of purified enzyme, specific activity for purified enzyme is 0.2578 U mg^{-1}.

4.2.4. G237S *Mt*CDH

Instead of metal caps and cotton plugs used in last fermentations, two-layer sterile gauze were used and showed better results related to wet biomass concentration of 63.4 g L^{-1} with an external protein concentration of 0.40 g L^{-1} (determined with the Bradford assay) and a volumetric DCIP activity of 0.1210 U mL^{-1} and a volumetric cytochrome *c* activity of 0.0085 U mL^{-1} (Figure 20).

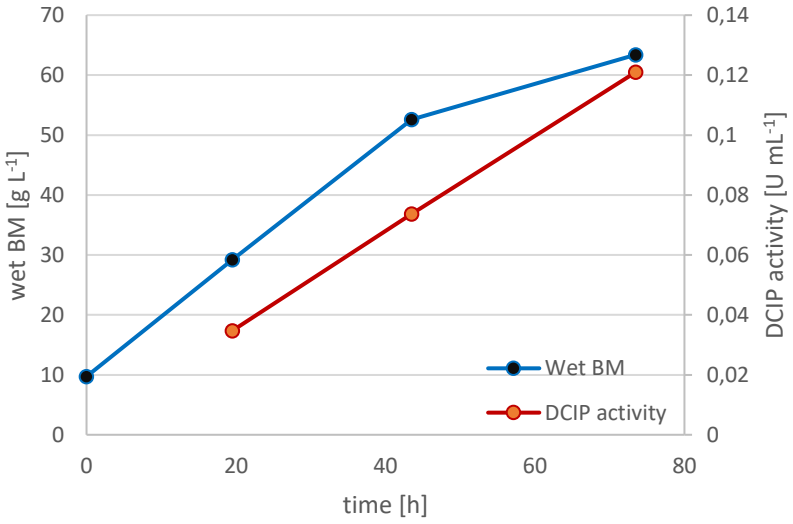

Figure 20. Production of the G237S *Mt*CDH in shaking flasks with curves for wet biomass concentration and DCIP activity

Two-step purification protocol is identical to the one used in G317S and G317A *Mt*CDH variant purification (see 4.2.2.). Only difference is multiple absorbance used during purification and peak detection. For first purification step 280 nm and 420 nm wavelengths were used while for second purification step absorbances for three different wavelengths were detected (280 nm, 420 nm and 450 nm), as it is shown in Figure 21. With the similar peak shape, same pooling technique and used wavelengths, the chromatograms below apply to the T306I variant as well.

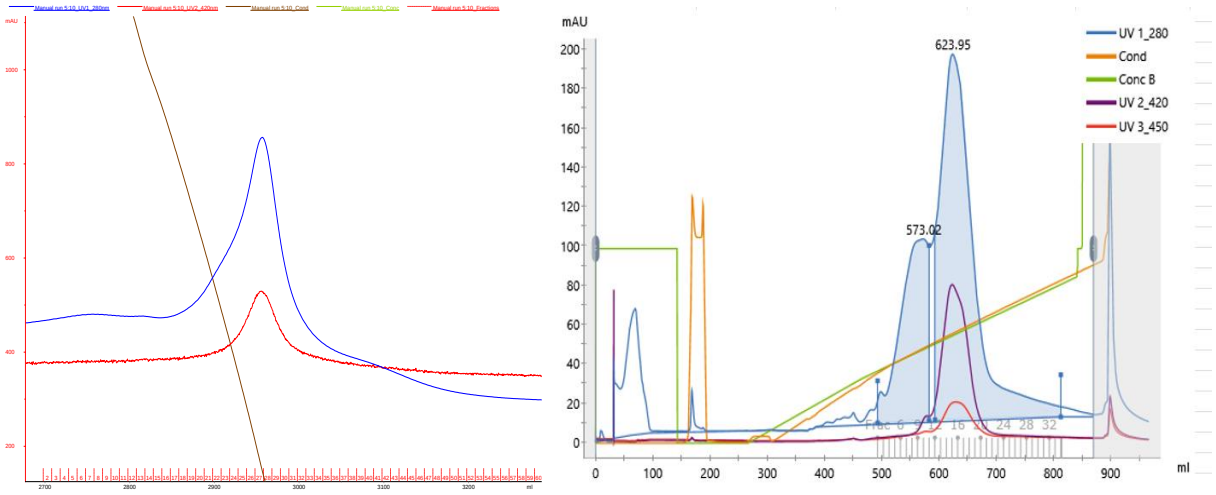

Figure 21. G237S *Mt*CDH purification chromatograms after two-step purification: HIC (left) and AEX (right).

A great benefit of multiple wavelengths usage is detection of heme and FAD domain, assuming of the presence of full-length enzyme. Proteins were collected in 10 mL fractions and strictly pooled. Target fractions were subjected to SDS-PAGE, and volumetric activities were measured

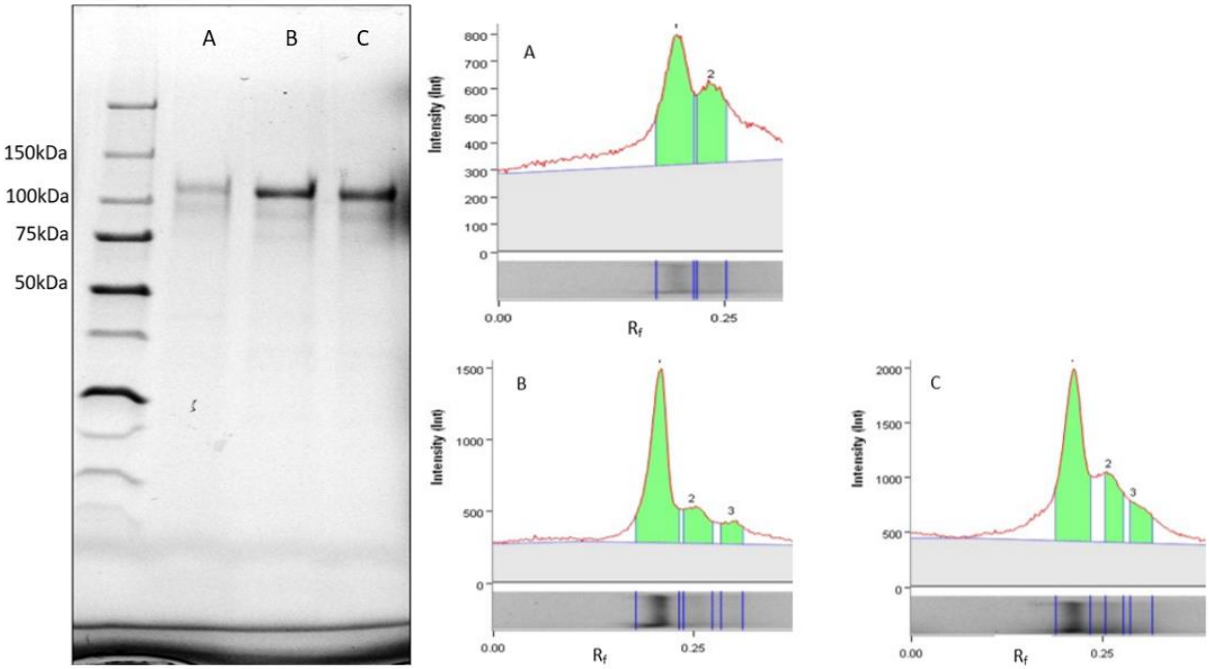

Figure 22. SDS-PAGE of HIC and AEX fractions (left) and lane and band analysis by Imager ChemiDoc^{TM} XRS+ 5.2.1. Imager Software for AEX band (right). Bands analyzed: pooled HIC fractions (A), AEX fraction 15 (B) and AEX pooled fractions

As it was assumed, lane and band analysis confirmed the highest purity of Band B of 72.1 %, and the lowest for HIC pooled fraction of 60.9 % (Figure 22). The 67.2 % purity of AEX pooled is comparable to the purity of 66.7 %, determined spectrophotometrically (A420/A280 nm ratio). Except from band identification, Imager Software is very useful tool for purity detection. With values like spectrophotometrically ones, it can be used as an alternative method for determining enzyme purity.

Table 12. Purification scheme for G237A *Mt*CDH and comparison within DCIP and cytochrome *c* assays, used for volumetric activity measurements

G237S	**Vol. activity (DCIP)**	**Protein conc.**	**Spec. activity**	**Volume**	**Total activity**	**Total protein**	**Yield**	**Purification level**
Step	U mL^{-1}	mg mL^{-1}	U mg^{-1}	mL	U	mg	%	
Supernatant	0.1210	0.40	0.2995	835	101.04	337.34	100	1
HIC	0.2298	0.65	0.3530	170	39.07	110.67	38.7	1.18
AEX	3.8750	5.24	0.7401	4.5	17.44	23.56	17.3	2.47

G237S	**Vol. activity (cyt *c*)**	**Protein conc.**	**Spec. activity**	**Volume**	**Total activity**	**Total protein**	**Yield**	**Purification level**
Step	U mL^{-1}	mg mL^{-1}	U mg^{-1}	mL	U	mg	%	
Supernatant	0.0085	0.40	0.0211	835	7.12	337.34	100	1
HIC	0.0350	0.65	0.0538	170	5.96	110.67	83.6	2.55
AEX	0.9430	5.24	0.1801	4.5	4.24	23.56	59.6	8.53

After each step, volumetric activities (DCIP and cytochrome *c* activity assays) and protein concentrations were detected. With low overall yield of the purification (17.26 %) using DCIP as an electron acceptor, specific activity for purified enzyme is 0.7401 U mg^{-1} (Table 12). On the other hand, data provided from cytochrome *c* assay measurements show that almost 60 % of full-length enzyme is preserved during two-step purification.

4.2.5. T306I *Mt*CDH and D305A *Mt*CDH

Initial volume of 1000 mL from the beginning dropped up to 410 mL (Table 13) due to contamination in two baffled flasks. Volumetric activity during fermentation and after harvesting was considerably higher compared to previous fermentation, and assuming on how much of protein will remain at the end of purification, it was decided to carry out protein purification. The culture reached wet biomass concentration of 70.86 g L^{-1} with an external protein concentration of 0.24 g L^{-1} (determined with the Bradford assay) and a volumetric DCIP

activity of 0.138 U mL^{-1} and a volumetric cytochrome *c* activity of 0.02 U mL^{-1} (Figure 23). Two-step purification protocol is applied for T306I variant (4.2.1.2.).

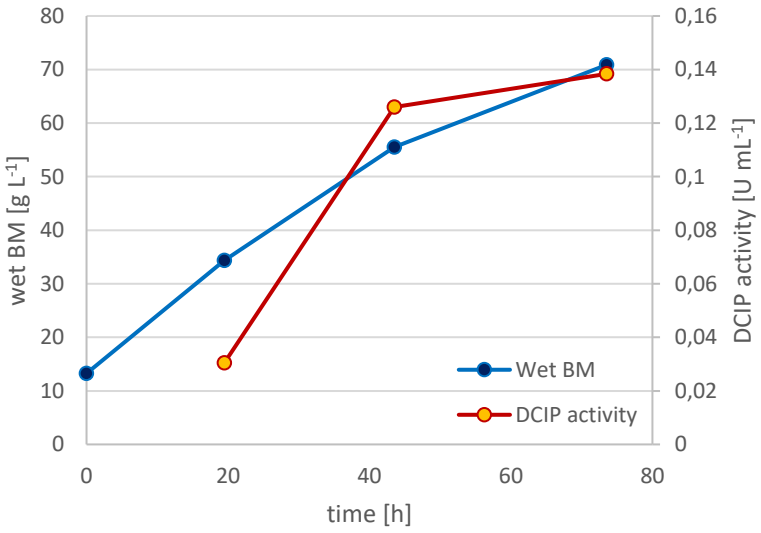

Figure 23. Production of the T306I *Mt*CDH in shaking flasks with curves for wet biomass concentration and DCIP activity

Table 13. Purification scheme for T306I *Mt*CDH and comparison within DCIP and cytochrome *c* assays, used for volumetric activity measurements

T306I	**Vol. activity (DCIP)**	**Protein conc.**	**Spec. activity**	**Volume**	**Total activity**	**Total protein**	**Yield**	**Purification level**
Step	U mL^{-1}	mg mL^{-1}	U mg^{-1}	mL	U	mg	%	
Supernatant	0.138	0.24	0.575	410	56.58	98.40	100	1
HIC	0.141	0.4339	0.326	120	16.97	52.07	30	0.57
AEX	2.622	2.0047	1.308	2.5	6.56	5.01	11.6	2.27

T306I	**Vol. activity (cyt *c*)**	**Protein conc.**	**Spec. activity**	**Volume**	**Total activity**	**Total protein**	**Yield**	**Purification level**
Step	U mL^{-1}	mg mL^{-1}	U mg^{-1}	mL	U	mg	%	
Supernatant	0.020	0.24	0.082	410	8.10	98.40	100	1
HIC	0.035	0.4339	0.081	120	4.24	52.07	52.4	0.99
AEX	1.259	2.0047	0.628	2.5	3.15	5.01	38.9	7.63

After each step, volumetric activities (DCIP and cytochrome *c* activity assays) and protein concentrations were detected. Specific activity (DCIP) for purified enzyme is 1.308 U mg^{-1}, was determined for pure enzyme. Before it was analyzed, pooled HIC fraction was stored much longer in 4 °C compared to other enzymes, which could reflect on decreased volumetric and specific activity, respectively.

4.2.6. D305A *Mt*CDH

The culture reached wet biomass concentration of 66.13 g L^{-1} with a volumetric DCIP activity of 0.162 U mL^{-1} and a volumetric cytochrome *c* activity of 0.005 U mL^{-1} (Figure 24).

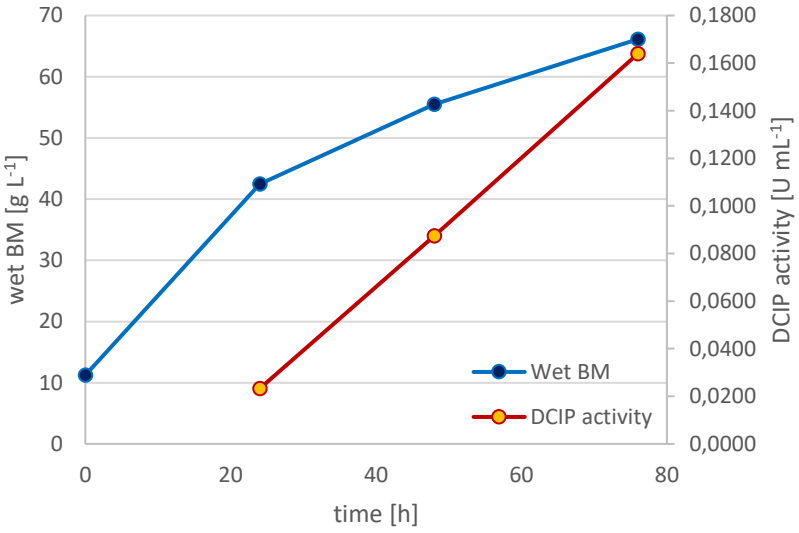

Figure 24. Production of the D305A *Mt*CDH in shaking flasks with curves for wet biomass concentration and DCIP activity

Two-step purification protocol is applied for D305A variant (4.2.1.2.). Compared to other purifications, "shoulder" of the main peak is detected during first and second purification step (Figure 25).

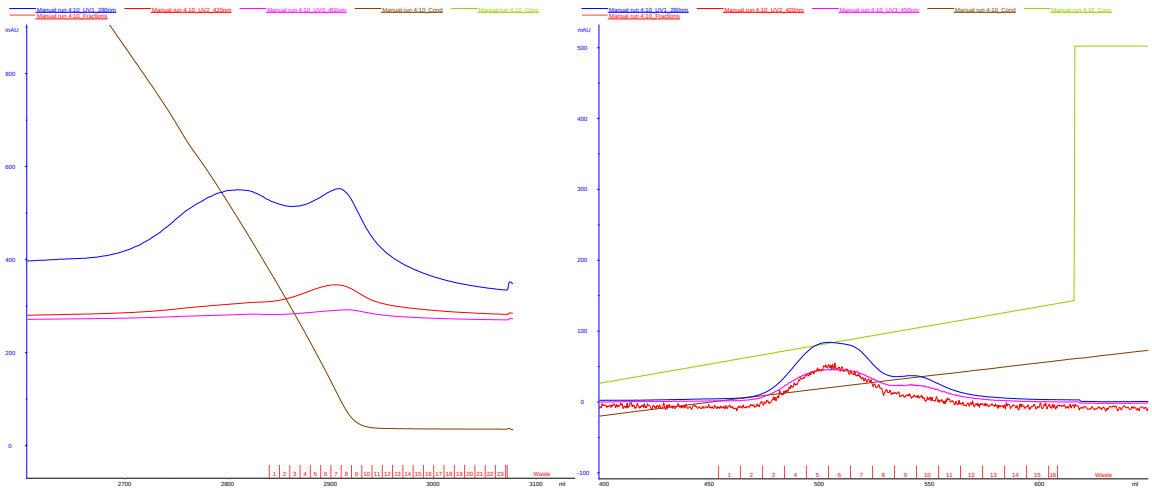

Figure 25. D305A *Mt*CDH purification chromatograms after two-step purification: HIC (left) and AEX (right)

Yield after first-purification step drastically dropped to 16.5 % (DCIP assay), as it is shown in Table 14, because only fractions in which all three absorptions appeared simultaneously were pooled. Nevertheless, since detected volumetric activity was lower than in supernatant, same scenario as with T306I is possible and these results shouldn't be considered with a high percentage of certainty. On the other hand, cytochrome *c* activity assay shows that the majority of produced two-domain enzyme was pooled and gives more reliable results.

Table 14. Purification scheme for D305A *Mt*CDH and comparison within DCIP and cytochrome *c* assays, used for volumetric activity measurements

D305A	**Vol. activity (DCIP)**	**Protein conc.**	**Spec. activity**	**Volume**	**Total activity**	**Total protein**	**Yield**	**Purification level**
Step	U mL^{-1}	mg mL^{-1}	U mg^{-1}	mL	U	mg		
Supernatant	0.162	0.340	0.477	715	115.97	243.10	100	1
HIC	0.137	0.567	0.241	140	19.14	79.38	16.5	0.51
AEX	2.335	2.518	0.928	3	7.01	7.55	6	1.94

D305A	**Vol. activity (cyt *c*)**	**Protein conc.**	**Spec. activity**	**Volume**	**Total activity**	**Total protein**	**Yield**	**Purification level**
Step	U mL^{-1}	mg mL^{-1}	U mg^{-1}	mL	U	mg		
Supernatant	0.005	0.340	0,015	715	3,52	243.10	100	1
HIC	0.024	0.567	0,042	140	3,33	79.38	94.5	2.89
AEX	0.706	2.518	0,281	3	2,12	7.55	60.1	19.35

4.3. EXPRESSION IN BIOFLO FERMENTER AND ENZYME PURIFICATION

4.3.1. Fermentation of G317S *Mt*CDH

Large-scale production of G317S *Mt*CDH was performed in a 5-L BioFlo fermenter (Figure 27). The cultivation was monitored for wet biomass, protein concentration and enzymatic activity. For the methanol feeding phase, a pulsed feed program was used. The fermentation was stopped after a total cultivation time of 120 h (94 h on methanol). At that time the culture reached a wet biomass of 219.1 g L^{-1} and an extracellular protein concentration of 0.51 g L^{-1} (determined with the Bradford assay) with a volumetric DCIP activity of 0.243 U mL^{-1}. The production curve is shown in Figure 26.

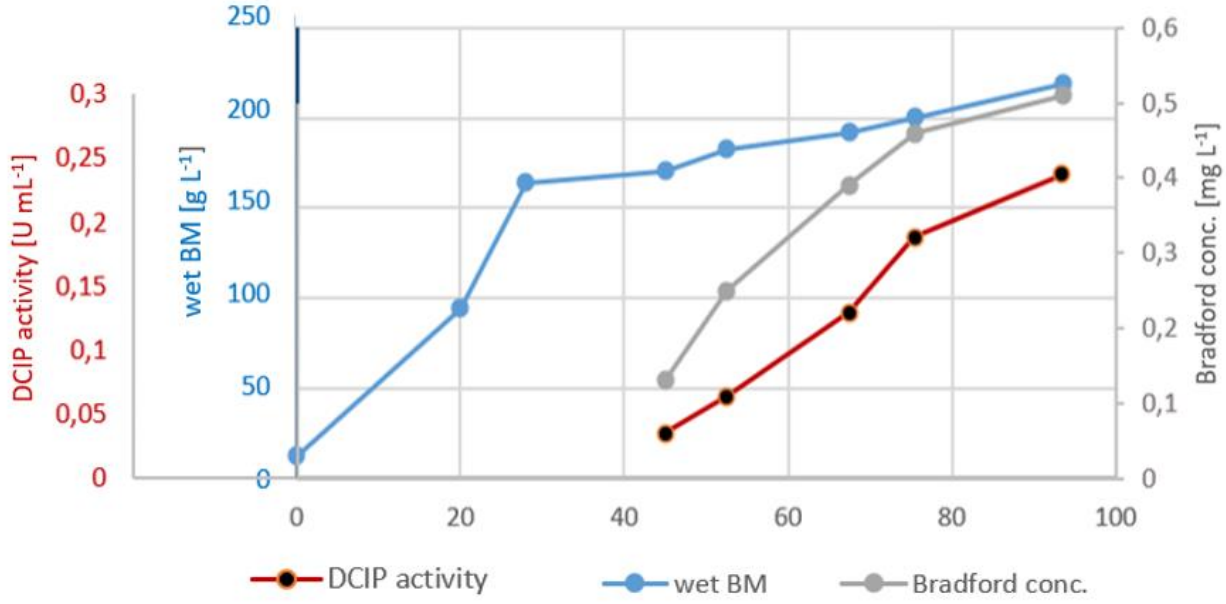

Figure 26. Production of the G317S *Mt*CDH variant in the bioreactor with curves for wet biomass concentration, protein concentration and DCIP activity

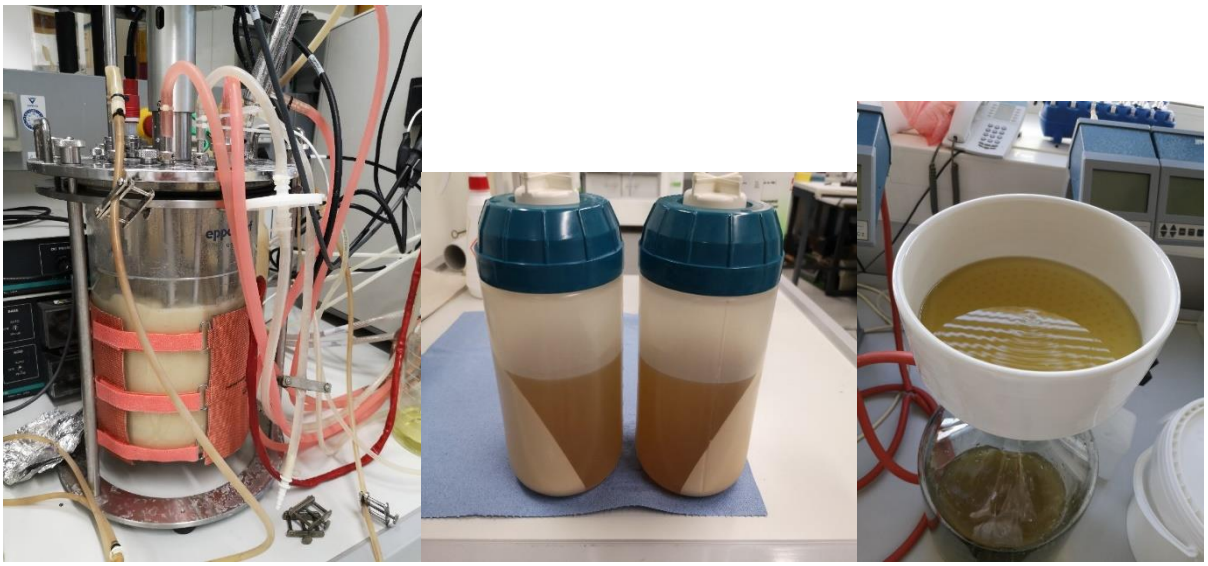

Figure 27. Fermentation in BioFlo bioreactor (left), medium after centrifugation (middle) and supernatant vacuum filtration (right)

4.3.2. Purification of G317S *Mt*CDH

The enzyme was purified using a two-step purification protocol including HIC and AEX. The first purification step (HIC) was performed on a Phenyl Sepharose fast flow column. Hence UV/VIS detector was set to 280 nm only, volumetric activity with DCIP and cytochrome *c*, and 420/280nm ratio were measured for fractions in range from 76 (initial fraction of the absorbance peak) to fraction 20 (Figure 28). Fractions 91-92 and 2-18 were pooled (V_{tot}=190mL) and used for the second purification step (AEX). The other fractions were frozen and kept as back-up samples.

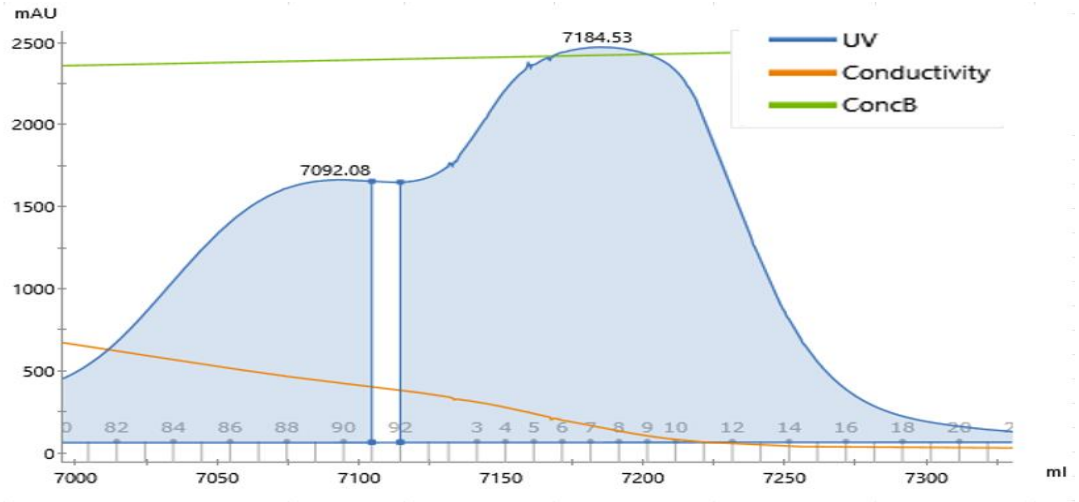

Figure 28. HIC Chromatogram for G317S *Mt*CDH (blue line shows absorption at 280 nm)

A buffer exchange of the pooled fractions to 20 mM HEPES pH 7.0 was performed using Amicon Ultra-15 centrifugal filters with a cut-off of 30 kDa until the conductivity was below 3 mS cm^{-1}. Then, the enzyme was loaded on a Source 30Q resin (52 mL) for the second purification step.

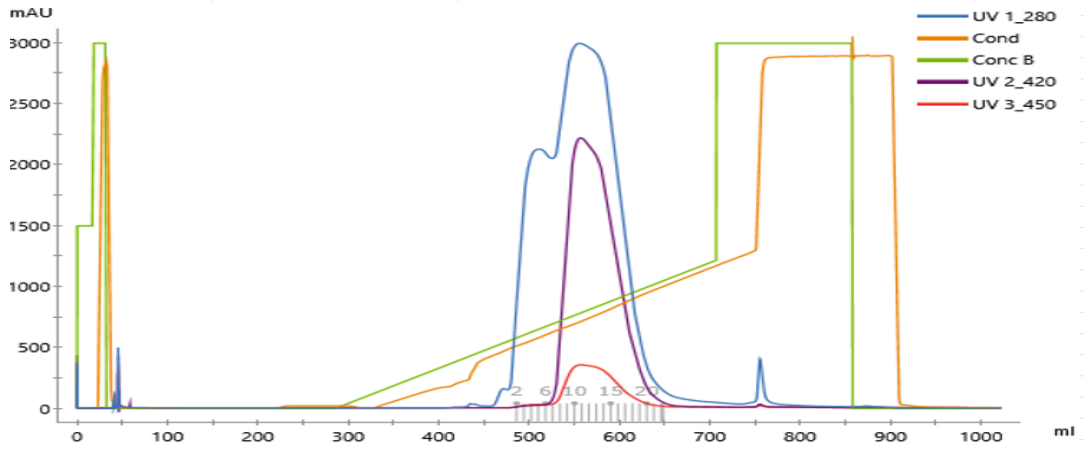

Figure 29. AEX Chromatogram for G317S *Mt*CDH

The UV/VIS detection for the second purification step was set to 280 nm, 420 nm and 450 nm in a way to detect protein, heme and flavin domain, respectively (Figure 29). Fraction 8-19 were detailly analyzed: volumetric activity (DCIP and cytochrome *c*), 420/280 nm ratio were detected (Table 15), and SDS-PAGE was performed. Overlaid spectra of target fractions with characteristic peaks are shown in Figure 30.

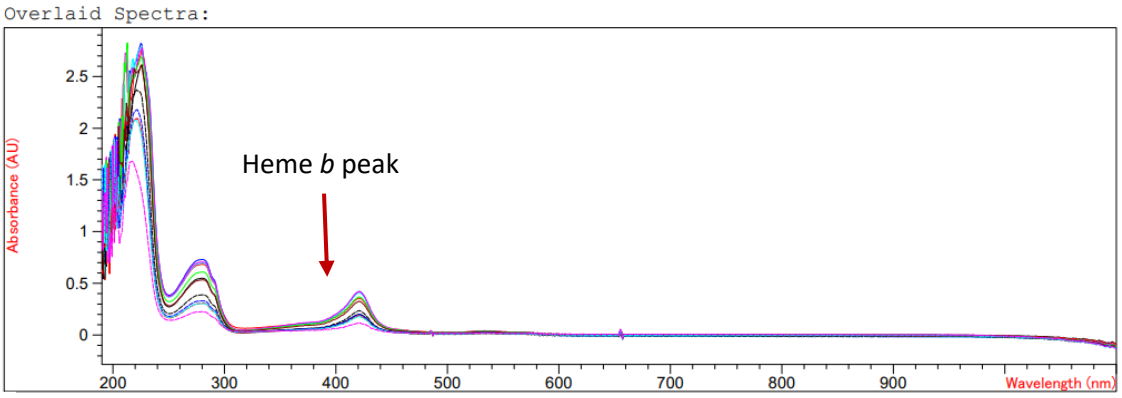

Figure 30. Overlaid spectra of AEX selected fractions (8-19) with characteristic peaks at 280 nm and 420 nm

Table 15. Concentration determination of AEX fractions

fraction	dilution	A_{280}	A_{420}	conc. (mg mL^{-1})	conc. (µM)	conc. (mg mL^{-1})	conc. (µM)	Ratio
				280 nm	280 nm	420 nm	420 nm	420/280
8	25	0.549	0.199	7.5	**86.4**	4.3	**49.8**	0.362
9	25	0.685	0.353	9.3	**107.7**	7.7	**88.4**	0.516
10	25	0.729	0.416	9.9	**114.6**	9.0	**104.0**	0.570
11	25	0.698	0.406	9.5	**109.7**	8.8	**101.7**	0.582
12	25	0.707	0.418	9.6	**111.2**	9.1	**104.6**	0.591
13	25	0.609	0.366	8.3	**95.7**	7.9	**91.6**	0.601
14	25	0.533	0.324	7.3	**83.9**	7.0	**81.0**	0.607
15	25	0.389	0.232	5.3	**61.1**	5.0	**58.0**	0.596
16	25	0.306	0.184	4.2	**48.1**	4.0	**46.1**	0.602
17	15	0.331	0.196	2.7	**31.2**	2.6	**29.5**	0.594
18	10	0.305	0.176	1.7	**19.2**	1.5	**17.6**	0.577
19	10	0.225	0.115	1.2	**14.1**	1.0	**11.5**	0.513

Fractions of the highest purity (11-17) were pooled, concentrated and rebuffered using Amicon Ultra-15 centrifugal filters with a cut-off of 30 kDa. G317S *Mt*CDH produced in BioFlo fermenter was used in presteady-state and steady-state measurements.

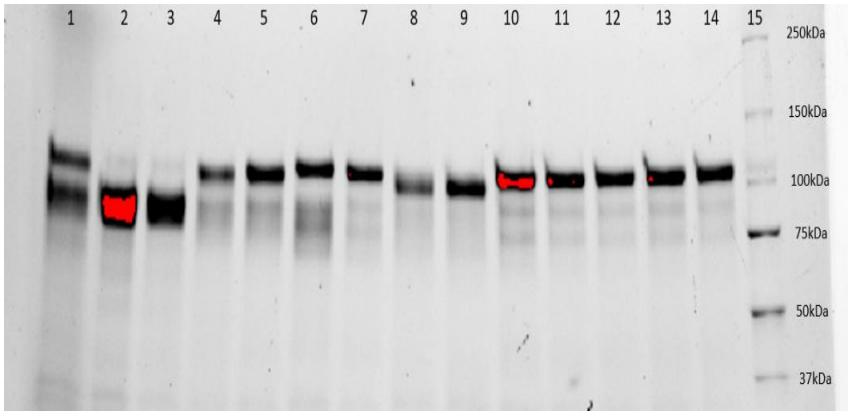

Sample	Fraction	Sample	Fraction
1	SUPERNATANT	9	AEX 18
2	HIC 88	10	AEX 10
3	HIC 18	11	AEX 11
4	HIC 14	12	AEX 12
5	HIC 7	13	AEX 13
6	AEX 8	14	AEX 14
7	AEX 9	15	marker
8	AEX 19		

Figure 31. SDS-PAGE of G317S *Mt*CDH samples after harvesting and two-step purification. Numbers next to HIC and AEX abbreviations correspond to fraction numbers (Figure 15 and Figure 16).

With the regard to the size of the enzyme, it was assumed that two bands detected in supernatant fraction represent two-domain glycosylated CDH and cleaved dehydrogenase domain (Figure 31). To confirm the presence of pure DH domain, DCIP and cytochrome *c* activity assays were performed. Single-band fractions *HIC 88* and *HIC 18*, yellow in color and

with only DCIP activity detected, are proved to be pure dehydrogenase domain. Figure 32 shows enzyme loaded on the column in the first step of purification, collected fractions after second step of purification and final concentrated enzyme solution.

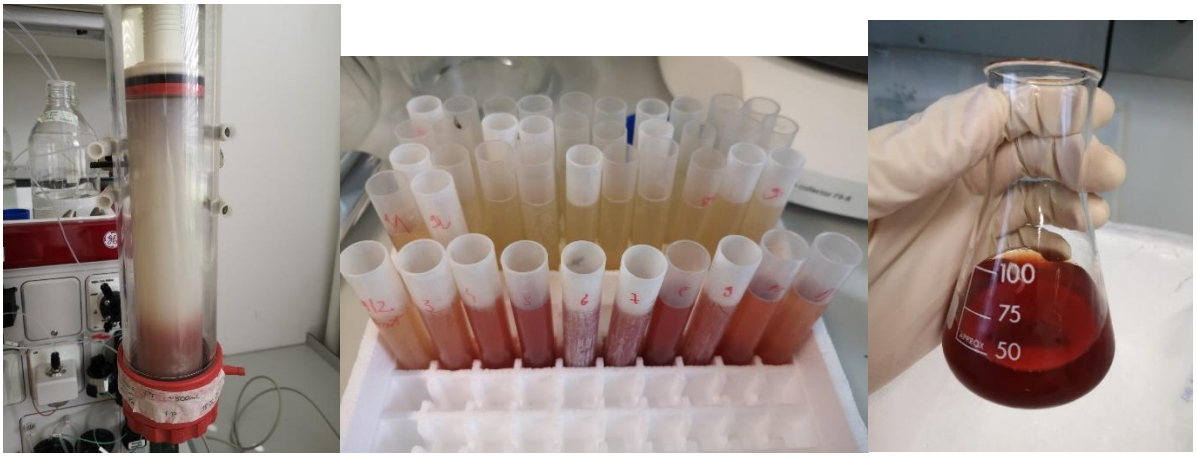

Figure 32. *Mt*CDH loaded on the Phenyl Sepharose FF column (left), collected fractions after AEX (middle) and final, concentrated enzyme solution (right)

4.4. CHARACTERIZATION

To characterize the purified variants, pH-profiles and temperature profiles with the substrate cellobiose were carried out. Furthermore, DSF, steady-state and presteady-state kinetic measurements were done. Purified enzymes with specific activities shown in Table 16 were used for further measurements and enzyme characterization.

Table 16. Specific activities of *Mt*CDH variants at pH 4.5 (sodium acetate buffer 100 mM) on cellobiose

	wild type	**G317S**	**G317A**	**G237S**	**T306I**	**D305A**
	Specific activity (U mg^{-1})					
DCIP assay	1.301	0.310	0.258	0.740	1.308	0.928
cyt *c* assay	0.397	0.082	0.084	0.181	0.628	0.281

4.4.1. pH profile

Table 17 shows the pH profiles of wild type and five produced and purified *Mt*CDH variants with cellulose as a natural substrate.

Table 17. Specific activities of variants in the pH range from 3.0 to 7.5 on cellobiose

pH	**Wild type**	**G317S**	**G317A**	**G237S**	**T306I**	**D305A**
	Specific activity [U mg^{-1}]					
3	0.467 ± 0.03	0.143 ± 0.01	0.151 ± 0.01	0.267 ± 0.01	0.521 ± 0.01	0.172 ± 0.01
3.5	0.709 ± 0.04	0.180 ± 0.01	0.184 ± 0.01	0.594 ± 0.03	1.031 ± 0.04	0.53 ± 0.02
4	1.078 ± 0.07	0.226 ± 0.01	0.239 ± 0.01	0.762 ± 0.01	1.485 ± 0.06	0.892 ± 0.02
4.5	1.304 ± 0.05	0.310 ± 0.01	0.309 ± 0.01	0.938 ± 0.02	2.013 ± 0.02	1.217 ± 0.05
5	1.502 ± 0.03	0.343 ± 0.01	0.371 ± 0.01	0.988 ± 0.04	2.190 ± 0.04	1.426 ± 0.03
5.5	1.598 ± 0.02	0.430 ± 0.02	0.435 ± 0.02	1.099 ± 0.03	2.514 ± 0.04	1.586 ± 0.04
6	1.626 ± 0.01	0.478 ± 0.02	0.473 ± 0.02	1.137 ± 0.02	2.528 ± 0.04	1.612 ± 0.04
6.5	1.303 ± 0.05	0.494 ± 0.04	0.513 ± 0.02	1.002 ± 0.02	2.134 ± 0.06	1.392 ± 0.03
7	0.797 ± 0.04	0.317 ± 0.01	0.335 ± 0.03	0.656 ± 0.02	1.346 ± 0.05	0.901 ± 0.02
7.5	0.431 ± 0.01	0.195 ± 0.01	0.231 ± 0.01	0.385 ± 0.02	0.768 ± 0.07	0.511 ± 0.03

According to the similar activity patterns, maximum specific activities are detected at pH 6.0: 1.626 U mg^{-1} for wild type, 1.137 U mg^{-1} for G237S, 2.528 U mg^{-1} for T306I and 1.612 U mg^{-1} for D305A variant. In comparison to mentioned variants, G237S and T306I share identical overall trend with slight decrease in activity at pH 5.0. Even though they share the lowest specific activities, pH-shift is detected for G317S and G317A variants, for which site-directed mutagenesis resulted in maximum reached activity at pH 6.5.

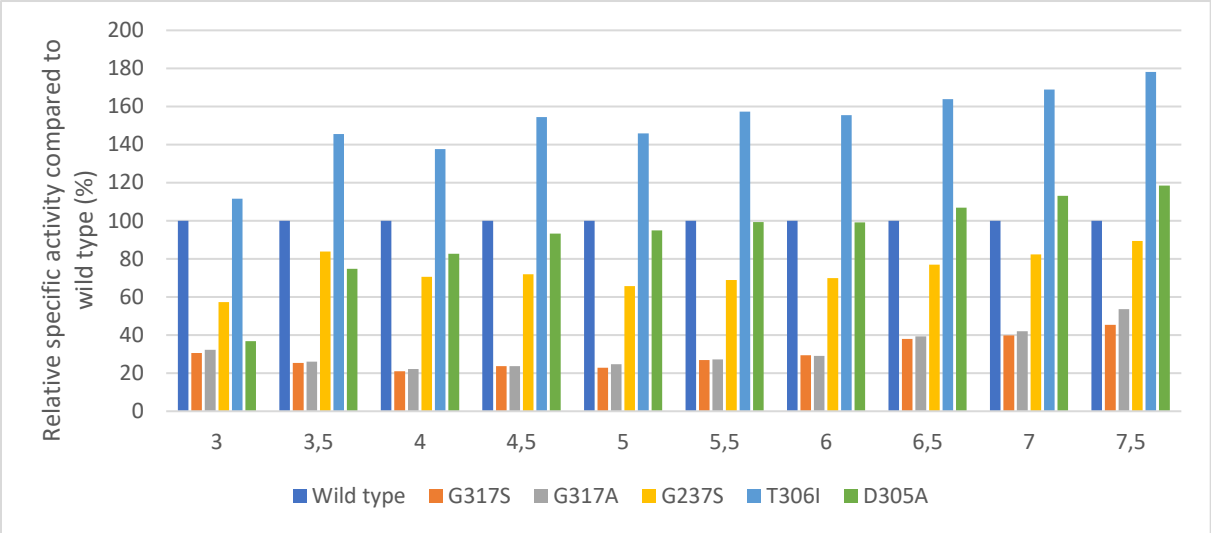

Figure 33. Specific activities of variants with cellobiose at different pHs compared to the wild-type activity. Wild type (dark blue bar) was set to 100 %

Relative activities of variants G317S, G317A and G237S are lower throughout whole pH range in comparison to the wild type. D305A shows higher values between pH 6.5 and pH 7.5., whereas relative specific activity of T306I is the highest in each pH point (Figure 33).

4.4.2. Thermal stability

The thermal stability curve shape of the G237S, T306I and D305A variants compared to the wild type is very similar with maximum activity reached at 37 °C. Variants G317S and G317A show a shifted temperature gradient profile with maximum specific activities at 50 °C (Figure 34).

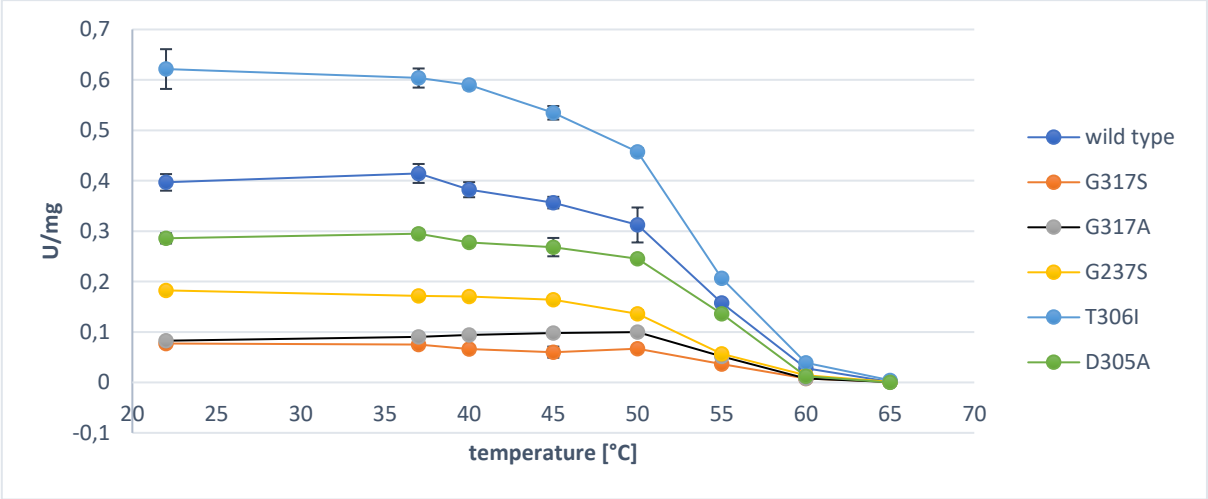

Figure 34. Temperature gradient stability: specific activities of variants and wild-type *Mt*CDH measured with cyt *c* at pH 4.5

4.4.3. Differential scanning fluorimetry (DSF)

Thermodynamic stabilities were measured by differential scanning fluorimetry (DSF) using a capillary-based instrument Prometheus NT.48 instrument (NanoTemper Technologies, US). Cellobiose dehydrogenase concentrations were adjusted to 2.0 mg mL^{-1} based on their molar absorption coefficients at 280 nm. Transition midpoint temperatures (T_m) of the enzymes were determined from the peak maximum of transition using the PR.Thermocontrol v.2.15 Software.

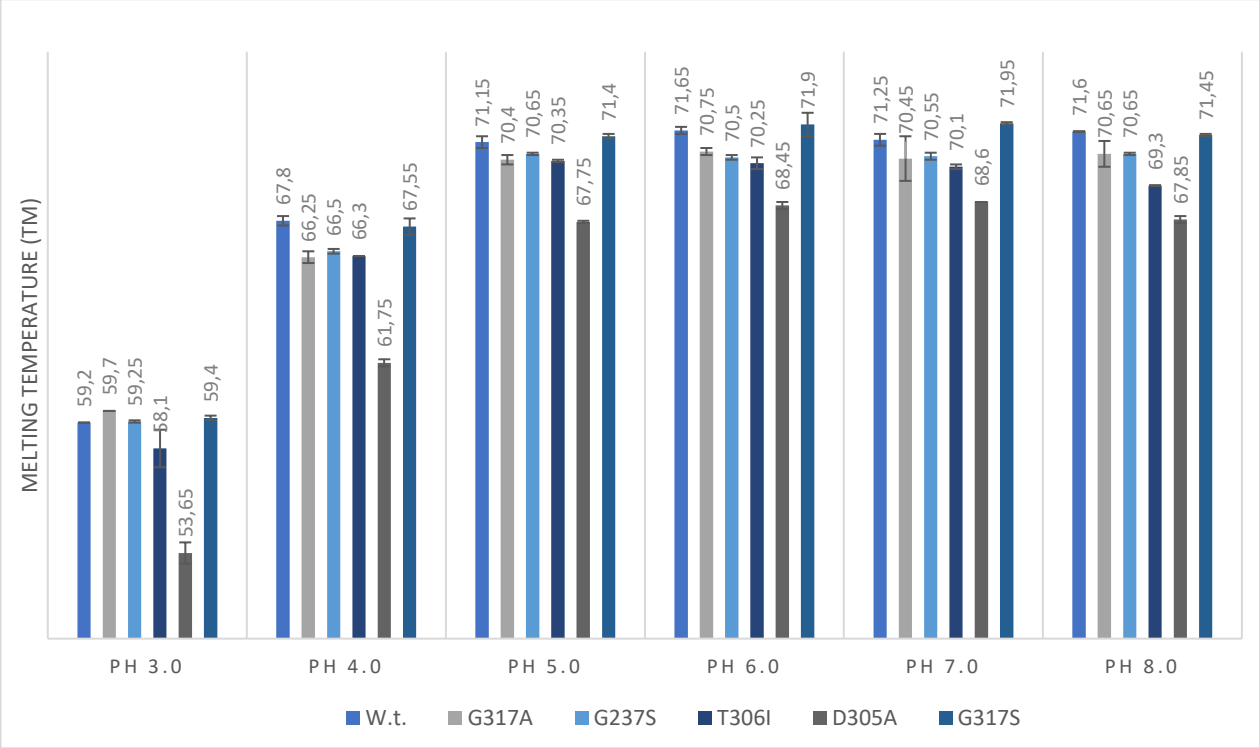

Figure 35. Melting points (T_m) for wild type and variants from pH 3.0 to pH 8.0

The thermal stability of all variants except D305A, compared to the wild type is more or less the same. D305A shows significantly lower melting temperatures between pH 3.0 and pH 4.0 and at pH 8.0. G317S variant shows maximum melting points in pH range 5.0-8.0 and at temperature of 71.95 °C (pH 7.0) half of the protein population is unfolded. For other variants and wild type, maximum melting temperatures are reached at pH 6.0 (Figure 35).

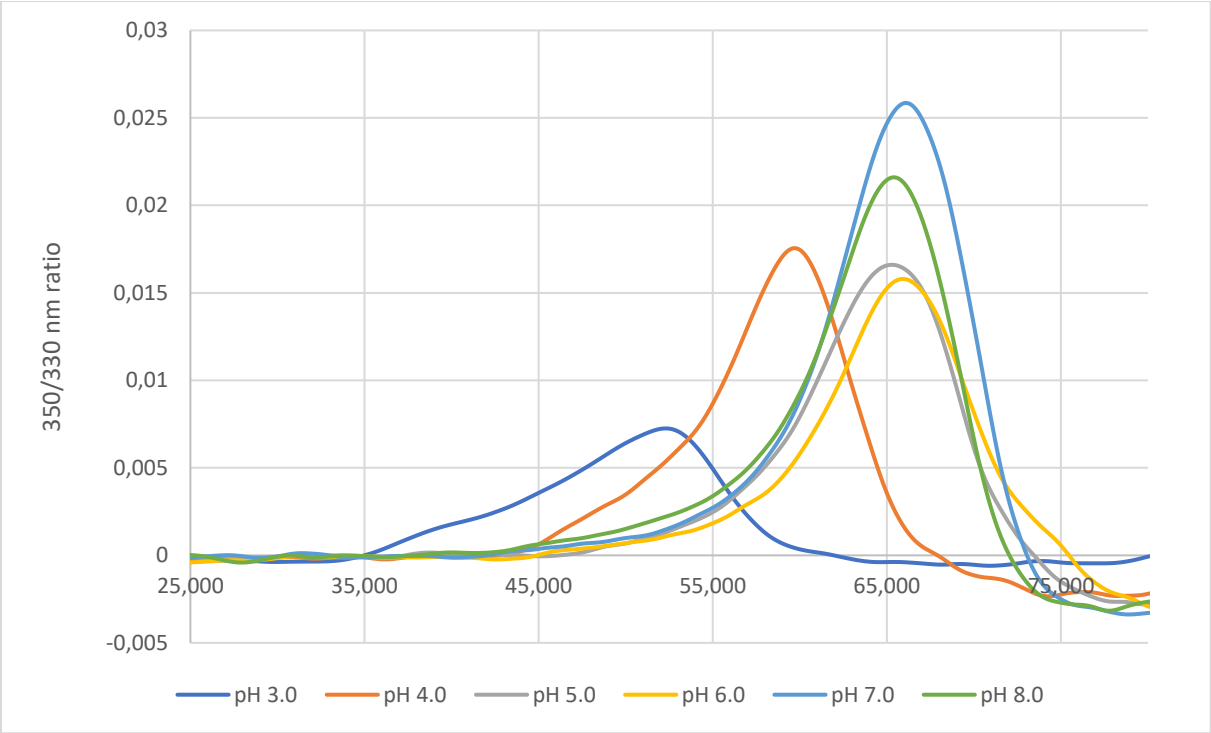

Figure 36. Example of a shifted temperature gradient profile for D305A variant between pH 3.0 and pH 8.0

The thermal stability of a protein is described by the thermal unfolding transition midpoint (T_m). In contrast to conventional DSF methods, nanoDSF uses tryptophan or tyrosine fluorescence to monitor protein unfolding. Both the fluorescence intensity and the fluorescence maximum strongly depend on the close surroundings of the tryptophan. Therefore, the ratio of the fluorescence intensities at 350 nm and 330 nm was suitable to detect any changes in protein structure, in our case protein unfolding. Only with these automatically calculated ratios it was possible to detect melting point for each analyzed sample. Even though the areas bellow the curve couldn't be compared (data not shown) all curves-combined graph (Figure 36) for each variant nicely shows shift in temperature gradient for different pH values.

4.4.4. Steady-state kinetic studies

The knowledge of the K_M value of an enzyme towards a particular substrate gives information on the approximation of substrate concentration in vivo. In this case, the K_M is equal to the dissociation constant of the ES complex, where a high K_M indicates weak binding, and a low K_M indicates strong substrate binding. Beside on the substrate converted, the K_M value for an enzyme depends on environmental conditions such as pH, temperature, and substrate concentration.

Catalytic constants K_m and V_{max} were determined from Michaelis-Menten curves (Figure 37) over a substrate range from 5.6 to 1200 µM cellobiose for all variants using 5 mM DCIP as electron acceptor. The reaction mixtures were buffered with 100 mM sodium-acetate buffer, pH 4.5 with measurements conducted in cuvettes. In comparison to one of the latest research with the same assay conditions (Flitsch et al., 2013), for which K_M and k_{cat} values for cellobiose were 35 µM and 4.11 s^{-1}, respectively, in this study K_M of 24.4 µM (1.45 times lower) and k_{cat} values of 1.96 s^{-1} were detected. From all kinetic data listed in Table 18, it is noticeable that the investigated CDH variants show low Michaelis-Menten constants, all of them in micromolar range from 16.96 (G237S) to 28.31 (T306I). In comparison to other substrates from literature, such as glucose, maltose, and lactose, all CDHs oxidize its natural substrate cellobiose more efficiently (Scheiblbrandner and Ludwig, 2019). The catalytic efficiencies (k_{cat}/K_m) vary from $2.27*10^3$ to $1.102*10^4$ M^{-1} s^{-1} with the lowest efficiency found for the G317S variant and the highest for the T306I variant. The catalytic efficiency for T306I variant has increased for 35.52 % compared to the wild type (Table 18). It is possible that the T306I mutation, close to the loop motif covering the FAD, stabilized the loop directly by filling gaps and therefore increased catalytic efficiency.

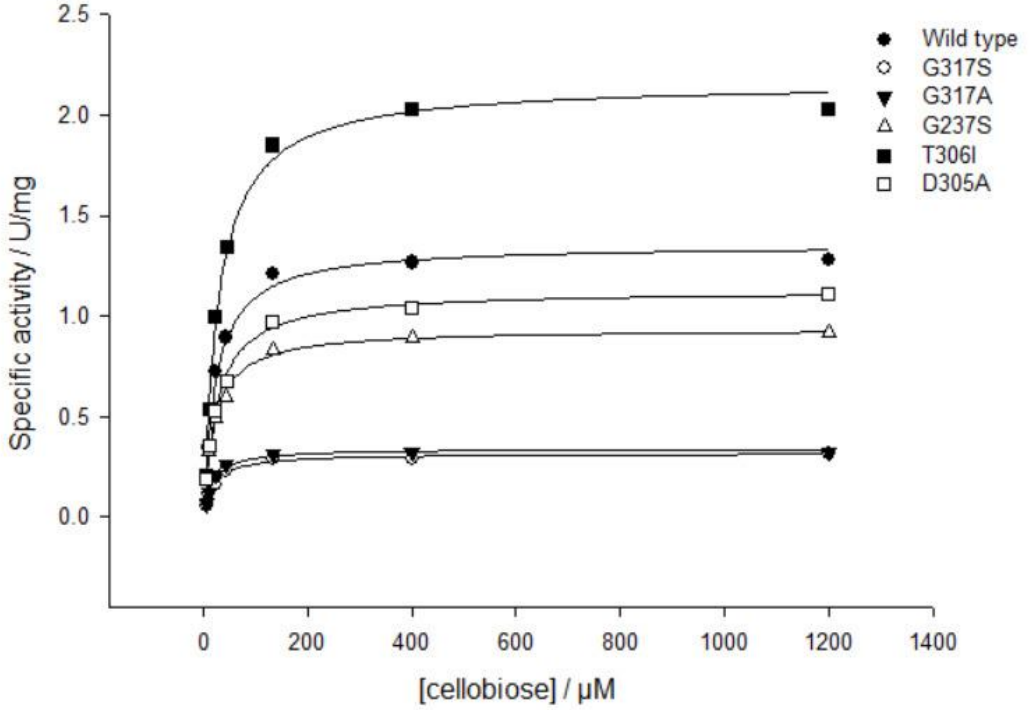

Figure 37. Michaelis-Menten curves used for the determination of kinetic constants of *Mt*CDH variants and wild-type

Table 18. Steady-state kinetic parameters of *Mt*CDH variants with DCIP as an electron acceptor and cellobiose as a substrate

Enzyme	K_m [µM]	V_{max} [U mg-1]	k_{cat} s^{-1}	k_{cat}/K_m [$M^{-1}s^{-1}$]
***Mt*CDH wild-type**	24.04 ± 3.44	1.354 ± 0.047	1.955	8131.42
***Mt*CDH G317S**	20.18 ± 2.09	0.317 ± 0.008	0.458	2269.31
***Mt*CDH G317A**	16.96 ± 2.45	0.341 ± 0.011	0.492	2901.05
***Mt*CDH G237S**	21.47 ± 1.32	0.936 ± 0.014	1.351	6294.46
***Mt*CDH T306I**	28.31 ± 3.61	2.161 ± 0.068	3.120	11019.88
***Mt*CDH D305A**	26.14 ± 1.63	1.127 ± 0.017	1.627	6224.44

The steady-state kinetic constants using DCIP as electron acceptor are an indicator for substrate turnover by the DH. As these mutations are close to the FAD, significant alterations in the substrate turnover rates were expected. Unfortunately, introduced mutations decreased catalytic efficiency. G237S variant, with mutation close to the FAD, shares similar constants with D305A variant. Thus, the results of each variant are in a good agreement with its corresponding mutation. To fully explain the influence of the mutations on the reaction mechanism, presteady-state experiments were performed, as summarized in the next section.

4.4.5. Presteady-state kinetics

In a stopped-flow apparatus, enzyme and the substrate are held in separate syringes. Enzyme solutions with a A420/A280 ratios from Table 19 were used in presteady-state kinetics measurements. The two components are quickly brought together and mixed in an observation chamber. Change in absorbance is recorded and the kinetic trace analyzed to obtain appropriate rate constants. This stopped-flow approach yields a complete time course of events as the reaction is continuously monitored and allows the direct determination of intramolecular electron transfer (IET), measured by the rate constant for heme *b* reduction.

Table 19. Enzymes with a A420/A280 ratios subjected to pre steady-state analysis

	A420/A280 ratio
Wild type	0.56
G317S	0.60
G317A	0.47
G237S	0.40
T306I	0.47
D305A	0.52

Absorption changes at 449 nm and 563 nm (Figure 38) were used to monitor FAD and heme reduction, respectively, and the observed rates (k_{obs}) were estimated by fitting the experimental data to a single exponential curve.

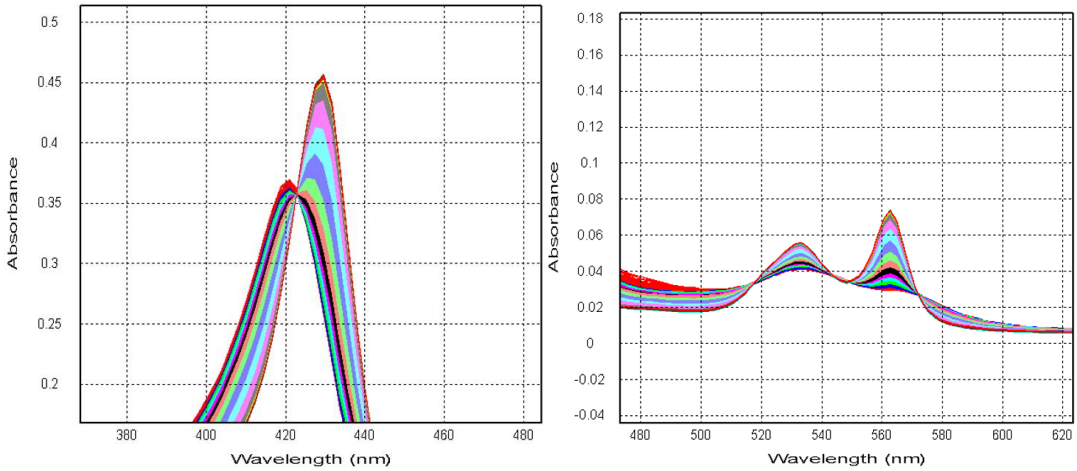

Figure 38. Presteady-state spectral changes of CDH upon mixing with cellobiose

Observed rate constant of the heme *b* for the wild-type CDH was 0.095 s^{-1}, whereas for FAD observed rate constant was 25.57 s^{-1} at pH 6.0. The 45 % and 48 % lower FAD-reduction rate indicate that G317S and G317A mutations have a negative impact on FAD-reduction. D305A and T306I variant share similar FAD-reduction rate while it is slightly decreased for G237S. In comparison to the FAD-reduction rates, mutations have similar effects on heme *b* reduction rates – large negative effects for G317S and G317A variants (up to 40 %) were detected, while G237S and D305A rates are close to the wild type. A notable exception is T306I, which shows similar FAD-reduction rate but the 16 % higher heme *b*-reduction rate (Figure 39). Since it is a loop mutation, it is possible that cytochrome domain was affected and consequently slightly alter interdomain electron transfer.

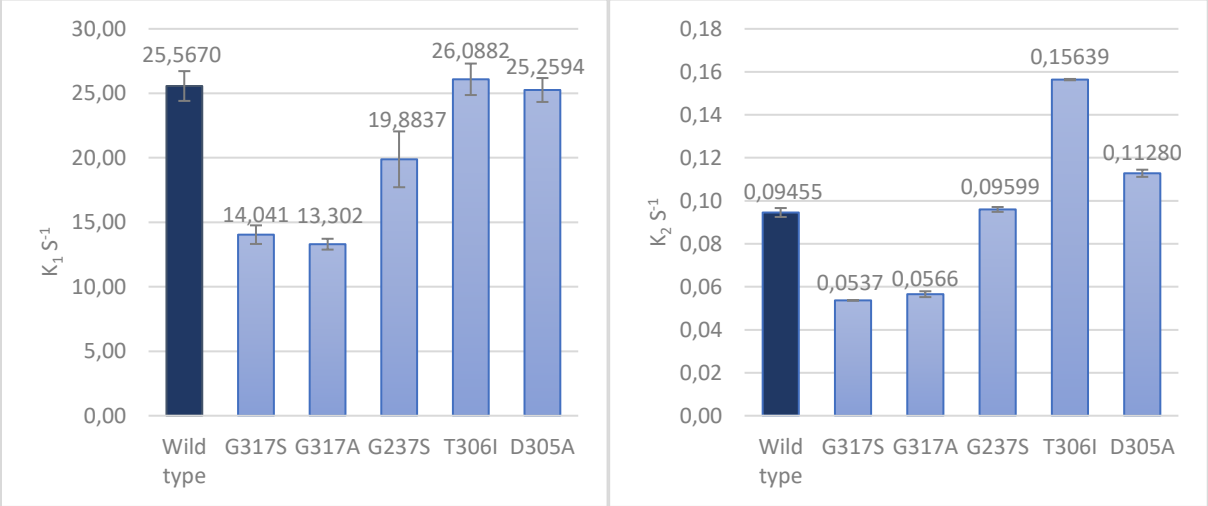

Figure 39. FAD and heme *b* reduction kinetics of *Mt*CDH wild type and variants. FAD reduction rates (left) are detected at 448.8nm and heme *b* reduction rates (right) at 562.9nm

The observed DET rates are turnover numbers (full cycle of CYT reduction and oxidation) determined under steady-state conditions and cannot be directly compared with the presteady-state IET rates (CYT reduction only) obtained by stopped-flow spectroscopy. Nevertheless, a rough comparison shows, that the DET rates are similar or higher than the IET rates which means that steady-state DET rate is faster and IET is rate limiting.

Given that the topic of the research has been relevant for past few years, there are not many references with which to compare the results obtained during this work.

5. CONCLUSIONS

1. Heterologous expression, purification and characterization of five *Mt*CDH cellobiose dehydrogenase variants in *Pichia pastoris* X-33 were successfully performed during this work.

2. Fermentation of *Mt*CDH variants in shaking flasks resulted in a low expression level with enzyme purities in the range from 67 to 86 % after a two-step chromatographical purification. With the aim of producing and isolating larger amounts of highly purified enzymes, fermentation in a 5-L BioFlo fermenter was carried out.

3. Fermentation process designed for the 5-L fermenter gives significantly better results and after identical purification protocol, two-domain enzyme with the RZ ratio of 0.6 ratio was isolated and used for presteady-state and steady-state kinetics measurements.

4. Mutations close to the FAD (G317S, G317A and G237S) resulted in significantly decreased specific activity, while T306I and D305A share almost the same specific activities.

5. G237S, T306I and D305A variants share similar pH and temperature profiles with wild-type *Mt*CDH. A pH-shift was detected for G317S and G317A variants, for which site-directed mutagenesis resulted in maximum reached activity at pH 6.5. Furthermore, these two show a shifted temperature gradient profile with maximum specific activities at 50 °C.

6. Thermodynamic stabilities were measured by differential scanning fluorimetry in which the transition midpoint temperature, in comparison to the wild-type, was only for G317S variant slightly altered. In general, results for wild-type and variants *Mt*CDH show the same stability trend i.e., the highest transition midpoint temperatures are between pH 5.0 and pH 7.0.

7. The catalytic efficiencies (k_{cat}/K_m) vary from $2.27*10^3$ to $1.102*10^4$ M^{-1} s^{-1} with the lowest efficiency found for the G317S variant and the highest for the T306I variant. The catalytic efficiency for T306I variant has increased for 35.52 % compared to the wild-type. It is possible that the T306I mutation, close to the loop motif covering the FAD, stabilized the loop directly by filling gaps and therefore increased catalytic efficiency.

8. Presteady-state kinetics was observed, and FAD and heme reduction rates were similar (D305A) or significantly decreased (G317S and G317A) compared to the wild-type. A notable exception is T306I, which shows similar FAD-reduction rate but the 16 % higher heme *b*-reduction rate, indicating the improvement of interdomain electron transfer.

9. Based on increased specific activity, catalytic efficiency, heme reduction rate and melting temperatures in the pH range from 5.0 to 8.0, the T306I variant seems to be the most promising variant for further investigation. Furthermore, kinetic stability of *Mt*CDH could be measured under turnover conditions and detect whether this variant could perform in a biosensor for extended time periods.

6. REFERENCES

Bissaro B, Várnai A, Røhr ÅK, Eijsink VGH (2018) Oxidoreductases and reactive oxygen species in conversion of lignocellulosic biomass. *Microbiol Mol Biol R* **82**, e00029-18. http://doi.org/10.1128/mmbr.00029-18

Bollella P, Gorton L, Ludwig R, Antiochia R (2017) A third generation glucose biosensor based on cellobiose dehydrogenase immobilized on a glassy carbon electrode decorated with electrodeposited gold nanoparticles: Characterization and application in human saliva. *Sensors* **17(8)**, 1912. http://doi.org/10.3390/s17081912

Buser C (2010) Toward sub-second correlative light and electron microscopy of *Saccharomyces cerevisiae*. *Method Cell Biol* **96**, 217–234. http://doi.org/10.1016/s0091-679x(10)96010-x

Cámara E, Landes N, Albiol J, Gasser B, Mattanovich D, Ferrer P (2017) Increased dosage of AOX1 promoter-regulated expression cassettes leads to transcription attenuation of the methanol metabolism in *Pichia pastoris*. *Sci Rep-UK* **7(1)**, 44302. http:/doi.org/10.1038/srep44302

Cameron MD, Aust SD (2001) Cellobiose dehydrogenase–an extracellular fungal flavocytochrome. *Enzyme Microb Tech* **28**, 129–138. http://doi.org/10.1016/s0141-0229(00)00307-0

Cavener DR (1992) GMC oxidoreductases: A newly defined family of homologous proteins with diverse catalytic activities. *J Mol Biol* **223**, 811–814. https://doi.org/10.1016/0022-2836(92)90992-S

Cereghino JL, Cregg JM (2000) Heterologous protein expression in the methylotrophic yeast *Pichia pastoris*. *FEMS Microbiol Rev* **24**, 45–66. http://doi.org/10.1111/j.1574-6976.2000.tb00532.x

Dart ML, Machleidt T, Jost E, Schwinn MK, Robers MB, Shi C, et al. (2018) Homogeneous assay for target engagement utilizing bioluminescent thermal shift. *Acs Med Chem Lett* **9**, 546–551. https://doi.org/10.1021/acsmedchemlett.8b00081

DirectSens (2021) 3G Biosensors. <https://www.directsens.com/technology-biosensors/>. Visited on November 14, 2021.

DirectSens (2021) LactoSens R: Lactose biosensor assay kit system. <https://www.directsens.com/lactosens/>. Visited on November 14, 2021.

Falk M, Pankratov D, Lindh L, Arnebrant T, Shleev S (2014) Miniature direct electron transfer based enzymatic fuel cell operating in human sweat and saliva. *Fuel Cells* **14**, 1050–1056. http://doi.org/10.1002/fuce.201400037

Flitsch A, Prasetyo EN, Sygmund C, Ludwig R, Nyanhongo GS, Guebitz GM (2013) Cellulose oxidation and bleaching processes based on recombinant *Myriococcum thermophilum* cellobiose dehydrogenase. *Enzyme Microb Tech* **52**, 60–67. http://doi.org/10.1016/j.enzmictec.2012.10.007

Geiss AF, Reichhart TMB, Pejker B, Plattner E, Herzog PL, Schulz C, et al. (2021) Engineering the turnover stability of cellobiose dehydrogenase toward long-term bioelectronic applications. *Acs Sustain Chem Eng* **9**, 7086–7100. http://doi.org/10.1021/acssuschemeng.1c0116

Grand View Research (2021) Biosensors market size, share & trends analysis report by application (medical, agriculture, environment) by technology (thermal, electrochemical, optical), by end-use, by region, and segment forecasts, 2021 – 2028. <https://www.grandviewresearch.com/industry-analysis/biosensors-market>. Visited on November 14, 2021.

Hallberg BM, Bergfors T, Bäckbro K, Pettersson G, Henriksson G, Divne C (2000) A new scaffold for binding haem in the cytochrome domain of the extracellular flavocytochrome cellobiose dehydrogenase. *Structure* **8**, 79–88. http://doi.org/10.1016/s0969-2126(00)00082-4

Hallberg BM, Henriksson G, Pettersson G, Divne C (2002) Crystal structure of the flavoprotein domain of the extracellular flavocytochrome cellobiose dehydrogenase. *J Mol Biol* **315(3)**, 421–434. http://doi.org/10.1006/jmbi.2001.5246

Henriksson G, Johansson G, Pettersson G (2000) A critical review of cellobiose dehydrogenases. *J Biotechnol* **78**, 93–113. https://doi.org/10.1016/S0168-1656(00)00206-6

Hildén L, Johansson G, Pettersson G, Li J, Ljungquist P, Henriksson G (2000) Do the extracellular enzymes cellobiose dehydrogenase and manganese peroxidase form a pathway in lignin biodegradation? *FEBS Lett* **477**, 79–83. http://doi.org/10.1016/s0014-5793(00)01757-9

Invitrogen (2010) EasySelect Pichia Expression Kit, Carlsbad.

Karbalaei M, Rezaee SA, Farsiani H (2020) *Pichia pastoris*: A highly successful expression system for optimal synthesis of heterologous proteins. *J Cell Physiol* **235**, 5867-5881. http://doi.org/10.1002/jcp.29583

Kracher D, Ludwig R (2016) Cellobiose dehydrogenase: An essential enzyme for lignocellulose degradation in nature – A review / Cellobiosedehydrogenase: Ein essentielles Enzym für den Lignozelluloseabbau in der Natur – Eine Übersicht. *Die Bodenkultur: Journal of Land Management, Food and Environment.* **67**, 145–163. http://doi.org/10.1515/boku-2016-0013

Krainer FW, Capone S, Jäger M, Vogl T, Gerstmann M, Glieder CH, et al. (2015) Optimizing cofactor availability for the production of recombinant heme peroxidase in *Pichia pastoris*. *Microb Cell Fact* **14**, 4. http://doi.org/10.1186/s12934-014-0187-z

Kremer SM, Wood PM (1992) Production of Fenton's reagent by cellobiose oxidase from cellulolytic cultures of *Phanerochaete chrysosporium*. *Eur J Biochem* **208**, 807-814. http://doi.org/10.1111/j.1432-1033.1992.tb17251.x

Lehner D, Zipper P, Henriksson G, Pettersson G (1996) Small-angle X-ray scattering studies on cellobiose dehydrogenase from *Phanerochaete chrysosporium. BBA-Protein Struct M* **1293**, 161–169. http://doi.org/10.1016/0167-4838(95)00245-6

Life Science Market (2021) pPICZ A. <https://www.lifescience-market.com/plasmid-c-94/ppicz-a-p-126550.html>. Visited on November 23, 2021.

Ludwig R, Ortiz R, Schulz C, Harreither W, Sygmund C, Gorton L (2013) Cellobiose dehydrogenase modified electrodes: advances by materials science and biochemical engineering. *Anal Bioanal Chem* **405**, 3637–3658. http://doi.org/10.1007/s00216-012-6627-x

Ma S, Ludwig R (2019) Direct electron transfer of enzymes facilitated by cytochromes. *Chem Electro Chem* **6**, 958-975. http://doi.org/10.1002/celc.201900058

Mathews FS, Bethge PH, Czerwinski EW (1979) The structure of cytochrome b562 from *Escherichia coli* at 2.5 A resolution. *J Biol Chem* **254**, 1699–1706. http://doi.org/10.1016/s0021-9258(17)37829-8

Nandini S, Nalini S, Reddy MBM, Suresh GS, Melo JS, Niranjana P, et al. (2016) Synthesis of one-dimensional gold nanostructures and the electrochemical application of the nanohybrid containing functionalized graphene oxide for cholesterol biosensing. *Bioelectrochemistry* **110**, 79–90. http://doi.org/10.1016/j.bioelechem.2016.03

NanoTemper Technologies (2015) Prometheus NT.48 – Product Information

Ortiz R, Rahman M, Zangrilli B, Sygmund C, Micheelsen PO, Silow M, et al. (2017) Engineering of cellobiose dehydrogenases for improved glucose sensitivity and reduced maltose affinity. *Chemelectrochem* **4**, 846–855. http://doi.org/10.1002/celc.201600781

Ozimek P, Veenhuis M, Vanderklei I (2005) Alcohol oxidase: A complex peroxisomal, oligomeric flavoprotein. *FEMS Yeast Res* **5**, 975–983. http://doi.org/10.1016/j.femsyr.2005.06.005

Pereira AR, Sedenho GC, Souza JCPD, Crespilho FN (2018) Advances in enzyme bioelectrochemistry. *An Acad Bras Cienc* **90**, 825-857. http://doi.org/10.1590/0001-3765201820170514

Rasala BA, Mayfield SP (2014) Photosynthetic biomanufacturing in green algae; production of recombinant proteins for industrial, nutritional, and medical uses. *Photosynth Res* **123**, 227–239. http://doi.org/10.1002/jcp.29583

Rotsaert FAJ, Li B, Renganathan V, Gold MH (2001) Site-directed mutagenesis of the heme axiallLigands in the hemoflavoenzyme cellobiose cehydrogenase. *Arch Biochem Biophys* **390**, 206–214. https://doi.org/10.1006/abbi.2001.2362

Santoso, A., Herawati, N., Rubiana, Y. (2012) Effect of methanol induction and incubation time on expression of human erythropoietin in methylotropic yeast *Pichia pastoris*. *Makara J Technol* **16**, 29–34. http://doi.org/10.7454/mst.v16i1.1041

Sassa A, Beard WA, Shock DD, Wilson SH (2013) *Steady-state*, pre-steady-state, and single-turnover kinetic measurement for dna glycosylase activity. *Jove-J Vis Exp* **78**, e50695. http://doi.org/10.3791/50695

Scheiblbrandner S (2012) Biochemical and electrochemical characterization of cellobiose dehydrogenase for application in glucose biosensors (Master thesis), University of Natural Resources and Applied Life Science, Vienna.

Scheiblbrandner, S, Ludwig, R (2019) Cellobiose dehydrogenase: Bioelectrochemical insights and applications. *Bioelectrochemistry* **131,** 107345. http://doi.org/10.1016/j.bioelechem.2019.107345

Stoica L, Ludwig R, Haltrich D, Gorton L (2006) Third-generation biosensor for lactose based on newly discovered cellobiose dehydrogenase. *Anal Chem* **78**, 393–398. http://doi.org/10.1021/ac050327o

Sützl L, Foley G, Gillam EMJ, Bodén M, Haltrich D (2019) The GMC superfamily of oxidoreductases revisited: analysis and evolution of fungal GMC oxidoreductases. *Biotechnol Biofuels* **12**, 118. https://doi.org/10.1186/s13068-019-1457-0

Sygmund C, Kittl R, Volc J, Halada P, Kubátová, E, Haltrich D, et al. (2008) Characterization of pyranose dehydrogenase from *Agaricus meleagris* and its application in the C-2 specific conversion of d-galactose. *J Biotechnol* **133**, 334–342. http://doi.org/10.1016/j.jbiotec.2007.10.013

Tan T-C, Kracher D, Gandini R, Sygmund C, Kittl R, Haltrich D, et al. (2015) Structural basis for cellobiose dehydrogenase action during oxidative cellulose degradation. *Nat Commun* **6**, 7542. http://doi.org/10.1038/ncomms8542

Wang J (2002) Glucose biosensors: 40 Years of advances and challenges. *Sensors* **10**, 107-119. http://doi.org/10.1002/1616-8984(200201)10:1<107::aid-seup107>3.0.co;2-q

Westermark U, Eriksson KE (1974) Cellobiose:quinone oxidoreductase, a new wood-degrading enzyme from white-rot fungi. *Acta Chem Scand* **28b**, 209–214.

Wong CM, Wong KH, Chen XD (2008) Glucose oxidase: natural occurrence, function, properties and industrial applications. *App Microbiol Biot* **78**, 927–938. http://doi.org/10.1007/s00253-008-1407-4

Wu S, Letchworth GJ (2004) High efficiency transformation by electroporation of *Pichia pastoris* pretreated with lithium acetate and dithiothreitol. *Biotechniques* **36**, 152–154. http://doi.org/10.2144/04361dd02

Yoo E-H, Lee S-Y (2010) Glucose biosensors: an overview of use in clinical practice. *Sensors* **10**, 4558–4576. http://doi.org/10.3390/s100504558

Zamocky M, Ludwig R, Peterbauer C, Hallberg B, Divne C, Nicholls P, et al. (2006) Cellobiose Dehydrogenase – A flavocytochrome from wood-degrading, phytopathogenic and saprotropic fungi. *Curr Protein Pept Sc* **7**, 255-280. http://doi.org/10.2174/138920306777452367

Zhang W, Li G (2004) Third-generation biosensors based on the direct electron transfer of proteins. *Anal Sci* **20**, 603–609. http://doi.org/10.2116/analsci.20.603

DECLARATION OF ORIGINALITY

I MARIO ILIĆ declare that this master's thesis is an original result of my own work and it has been generated by me using no other resources than the ones listed in it.

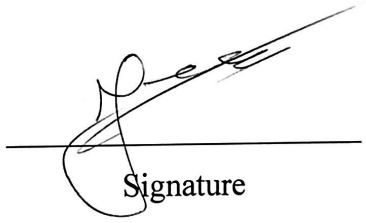

Signature